Macleans Nose, Sound of Mull

HYDRODYNAMIC MODELLING REPORT
05.18V3

[redacted]

[redacted]

TABLE OF CONTENTS

list Of Figures 3
List Of Tables 6
1. Introduction 7
2. Objectives Of The Modelling Study 7
2.1 Site Proposal 8
2.2 General Environmental Risks Associated With Aquaculture Discharges 8
3 Hydrodynamic Model Description And Configuration 11
3.1 Model Description 11
3.2 Calibration 15
4. Hydrodynamic Modelling Results 16
4.1 Calibration, May – July 2017 16
4.2 Validation, April – May 2010 21
4.2.1 Sea Surface Height 21
4.2.2 Velocity Time Series 23
4.3 Modelled Flow Fields 26
4.4 Preparing Velocity Data For Newdepomod 28
5. Newdepomod Modelling 29
5.1 Initial Testing 29
5.2 Calibration And Validation Simulations 29
5.3 Model Inputs And Flow Fields 30
5.3.1 Wind Forcing 30
5.3.2 Flow Fields, 18th January – 5th May 2017 32
5.3.3 Flow Fields, 30th October 2015 – 12th February 2016 34
5.3.4 Waste Feed And Faecal Solids 35
5.4 Calibration And Validation Results 37
5.4.1 Slice ("Embz") 37
5.4.2 Benthic Footprint ("None"), October 2016 – May 2017 40
5.4.3 Benthic Footprint ("None"), July 2015 – February 2016 43
5.4.4 Benthic Footprint ("None"), October 2016 – October 2017 44
6. Newdepomod Forecasting 45
References 46

LIST OF FIGURES

Figure 1. The proposed configuration of cages at Macleans Nose. 8

Figure 2. The unstructured mesh for the Loch Sunart/western Sound of Mull local area model. 12

Figure 3. The unstructured mesh around the Macleans Nose site, with the proposed cage layout indicated (o). 12

Figure 4. The WLLS model domain that provides boundary conditions for the Sunart/wSoM model (□) 13

Figure 5. Water depths (m) in the Sunart/wSoM local area model. 14

Figure 6. Water depths (m) in the Macleans Nose region. The locations of the north and south ADCP deployments (▲) and proposed cages (o) are shown. 14

Figure 7. Averaged flows from 9 rivers and streams entering Loch Sunart and the western Sound of Mull from the 30-year climatology used by the Scottish Shelf Model. The largest flow is from the Carnoch River at the head of Loch Sunart. 15

Figure 8. Comparison between observed and modelled sea surface height at the northern ADCP location from March - May 2017 with parameter values from Table 1. Both the full record (left) and a subset of 15 days (right) are shown. Observed data are in blue, modelled data in red.....17

Figure 9. Comparison between observed and modelled East (left) and North (right) components of near-surface (top), mid-depth (middle) and near-bed (bottom) velocity at the northern ADCP location in March – May 2017. Observed data are in blue, modelled data in red..... 18

Figure 10. Comparison between observed and modelled East (left) and North (right) components of near-surface (top), mid-depth (middle) and near-bed (bottom) velocity at the southern ADCP location in March – May 2017. Observed data are in blue, modelled data in red..... 18

Figure 11. Histograms of measured and modelled current speed (left) and direction (right) at near-surface (top), mid-depth (middle) and near-bed (bottom) depths for the north ADCP location during March – May 2017. 20

Figure 12. Histograms of measured and modelled current speed (left) and direction (right) at near-surface (top), mid-depth (middle) and near-bed (bottom) depths for the south ADCP location during March – May 2017. 21

Figure 13. Comparison between observed and modelled sea surface height at the northern ADCP location from May – July 2017 with parameter values from Table 1. Both the full record (left) and a subset of 15 days (right) are shown. Observed data are in blue, modelled data in red..... 22

Figure 14. Comparison between observed and modelled sea surface height at the southern ADCP location from May – July 2017 with parameter values from Table 1. Both the full record

(left) and a subset of 15 days (right) are shown. Observed data are in blue, modelled data in red..... 22

Figure 15. Comparison between observed and modelled East (left) and North (right) components of near-surface (top), mid-depth (middle) and near-bed (bottom) velocity at the northern ADCP location in May – July 2017. Observed data are in blue, modelled data in red. 23

Figure 16. Comparison between observed and modelled East (left) and North (right) components of near-surface (top), mid-depth (middle) and near-bed (bottom) velocity at the southern ADCP location in May – July 2017. Observed data are in blue, modelled data in red. 24

Figure 17. Histograms of measured and modelled current speed (left) and direction (right) at near-surface (top), mid-depth (middle) and near-bed (bottom) depths for the north ADCP location during May – July 2017. 25

Figure 18. Histograms of measured and modelled current speed (left) and direction (right) at near-surface (top), mid-depth (middle) and near-bed (bottom) depths for the south ADCP location during May – July 2017. 26

Figure 19. Modelled surface flood (top) and ebb (bottom) tide current vectors at spring tide on 28th April 2017. Every third vector is shown. 27

Figure 20. Modelled near-bed flood (top) and ebb (bottom) tide current vectors at spring tide on 28th April 2017. Every third vector is shown. 27

Figure 21. The NewDepomod unstructured mesh for Macleans Nose, with the proposed cage locations (o) and the locations of the FVCOM hydrodynamic model cell centres (·) indicated. 28

Figure 22. Hourly measured wind speed and direction from Tiree for the period 30th October 2015 – 12th February 2016. Data were only obtained for wind speeds exceeding 9 m s^{-1}. The direction data are in meteorological convention. 31

Figure 23. Hourly measured wind speed and direction from Tiree for the period 15th January – 6th May 2017. The direction data are in meteorological convention..... 31

Figure 24. Location (•) of the modelled time series in Figure 25..... 32

Figure 25. East (top) and North (bottom) components of the near-bed modelled flows, tide only (left) and full flow (right), for January – May 2017 at the Macleans Nose site (Figure 24). The time series length is 2568, corresponding to 107 days of hourly values. 33

Figure 26. Modelled surface flow fields at intervals through a tidal cycle on 28th April 2017 (spring tide). The velocity vectors are superimposed on the coloured current speed. High water was at 07:15 on 28th April 2017. 33

Figure 27. Modelled mean full flow current speed for surface (left) and nearbed (right) depths for January - May 2017. 34

Figure 28. East (top) and North (bottom) components of the modelled flows, for October 2015 – February 2016 at the Macleans Nose site (Figure 24). The record length is 2520, corresponding to 105 days of hourly values. 35

Figure 29. Modelled mean full flow current speed at surface (left) and near-bed (right) depths for October 2015 – February 2016. 35

Figure 30. Time series of waste feed and faecal solids supplied to NewDepomod for the 2016 – 2017 production cycle. The times of seabed surveys are indicated. 36

Figure 31. Time series of waste feed and faecal solids supplied to NewDepomod for the July 2015 – February 2016 simulation. The time of the seabed survey is indicated..... 37

Figure 32. Results of the Slice calibration for the survey of 3rd – 4th May 2017. Results from the run with SEPA default parameter settings are shown on top, results from the calibration simulation on the bottom. The modelled concentrations and sample locations are shown on the left, and the modelled and observed concentrations along the transect indicated are shown on the right..... 38

Figure 33. Results of the Slice validation for the survey of 11th February 2016. EmBZ concentrations are shown in plan view (left) and along the transect, from north to south (right). 40

Figure 34. Results of the Slice validation for the survey of 24th October 2017. EmBZ concentrations are shown in plan view (left) and along the transect, from north to south (right). 40

Figure 35. Results of the calibration for October 2016 – May 2017. The 80th percentile of deposition over the simulation period is shown with the sample locations indicated (left). On the right, the relationship between 80th percentile of deposition and the observed IQI is shown. The red line indicates the relationship between deposition and IQI used to forecast the future footprint. Note that deposition at Station 6 (green point) was poorly modelled, and that data point was not used when fitting the curve, but it was included when the errors (r2, RMSE) were calculated. 42

Figure 36. Modelled footprint, based on the 80th percentile of deposition (left), and predicted IQI against observed IQI (right) for February 2016. 43

Figure 37. Modelled footprint, based on the 80th percentile of deposition (left), and predicted IQI against observed IQI (right) for October 2017. 44

LIST OF TABLES

Table 1. Parameter values chosen for the FVCOM model during the calibration simulations. 16

Table 2. Model performance statistics for sea surface height (SSH) at the north and south ADCP locations from the selected calibration simulation, March – May 2017. 19

Table 3. Model performance statistics for east and north components of velocity at the north ADCP location from the selected calibration simulation, March – May 2017. 19

Table 4. Model performance statistics for east and north components of velocity at the south ADCP location from the selected calibration simulation, March – May 2017. 19

Table 5. Model performance statistics for sea surface height (SSH) at the north and south ADCP locations from the validation simulation, May – July 2017. 22

Table 6. Model performance statistics for east and north components of velocity at the north ADCP location from the validation simulation, May – July 2017. 24

Table 7. Model performance statistics for east and north components of velocity at the south ADCP location from the validation simulation, May – July 2017. 25

Table 8. Slice (active ingredient: emamectin benzoate, “EmBZ”) treatments and residue surveys during the 2015-16 and 2016-17 production cycles at Macleans Nose. 30

Table 9. NewDepomod parameter values that achieved the best calibration result. Values that are different from the SEPA default values are highlighted in bold. 39

Table 10. Observed Infaunal Quality Index (IQI) values at Macleans Nose at 16 stations sampled during 3rd – 5th May 2017. 41

Table 11. Observed Infaunal Quality Index (IQI) values at Macleans Nose at 6 stations sampled on 11th February 2016. 43

Table 12. Observed Infaunal Quality Index (IQI) values at Macleans Nose at 6 stations sampled on 24th October 2017. 44

1. INTRODUCTION

This report presents details of the hydrodynamic (HD) modelling undertaken to underpin the application of the particle-tracking model, (New)Depomod, to simulate the discharge, dispersion and fate of waste feed, faeces, and residues of the in-feed sea lice therapeutant, Slice, at a Marine Harvest (Scotland) (MHS) fish farm site at **Macleans Nose**. The overall purpose of the modelling is to adequately represent the coastal processes involved in particle transport in the near field and far field, and to inform and support the resulting CAR application. For applications where a biomass exceeding 2500 tonnes is requested, a detailed modelling study is required, including the use of a hydrodynamic model to describe the spatial variations in the current field in the region of the site, and to utilise these current fields in the application of NewDepomod.

This modelling report will focus on the hydrodynamic modelling undertaken as part of this application, including the following aspects of the modelling process:

- A description of the hydrodynamic model used, its configuration and boundary forcing;
- A description of the model grid and bathymetry in the region of the site;
- A description of the calibration and validation process undertaken;
- A description of the simulations run to force NewDepomod;
- A description of the configuration of, and simulations performed using, NewDepomod;

The observations used to calibrate and evaluate the model are described in separate hydrographic reports, and the results from the NewDepomod simulations are also summarised in a separate modelling report. The modelling methodology described here follows as closely as possible the modelling guidelines issued by the Scottish Environment Protection Agency (SEPA) in February 2018 (SEPA, 2018).

2. OBJECTIVES OF THE MODELLING STUDY

The modelling study is designed to simulate the release, dispersion and fate of waste particles from the cages to the immediate area beneath and around the cages, and to determine their dispersion over a larger domain. The fate of Slice residues will also be addressed. The modelling study will take cognisance of the existing cage set up and deposition on the sea bed. The existing suite of benthic data allows modelled benthic predictions to be calibrated against real data.

Two types of model will be described in this report: the hydrodynamic model and NewDepomod, a bespoke particle-tracking model. The models have been calibrated and have undergone validation runs, and were then used in a sequential manner. The hydrodynamic model was initially used to determine the maximum distance that particles released from the farm site will travel in all directions. This will dictate the size and shape of the study model domain for the particle tracking model. Current velocity fields were then extracted from the hydrodynamic model and used to provide input data to the particle tracking model, which was run to produce outputs of carbon deposition and in-feed sealice treatment concentrations.

The use of a hydrodynamic model to provide spatially varying current data, from multiple nodal points, provides an improved method of providing input data to the particle tracking model, as opposed to the use of a single fixed-location current meter. The outputs from the particle tracking model are summarised in a separate report as part of an application to SEPA for the cage site.

2.1 Site Proposal

The current site layout consists of twelve circular cages of 120m circumference and has a consented maximum biomass of 2500 tonnes. The cages are in two groups, each in a 3x2 array, with 14 m deep nets. The current proposal is to increase the number of cages to up to 16 x 120 m circumference, by adding up to 4 cages to the southeast (Figure **1**). The biomass requested will depend on the outcome of the modelling process, but a biomass of about 3500 tonnes is targeted.

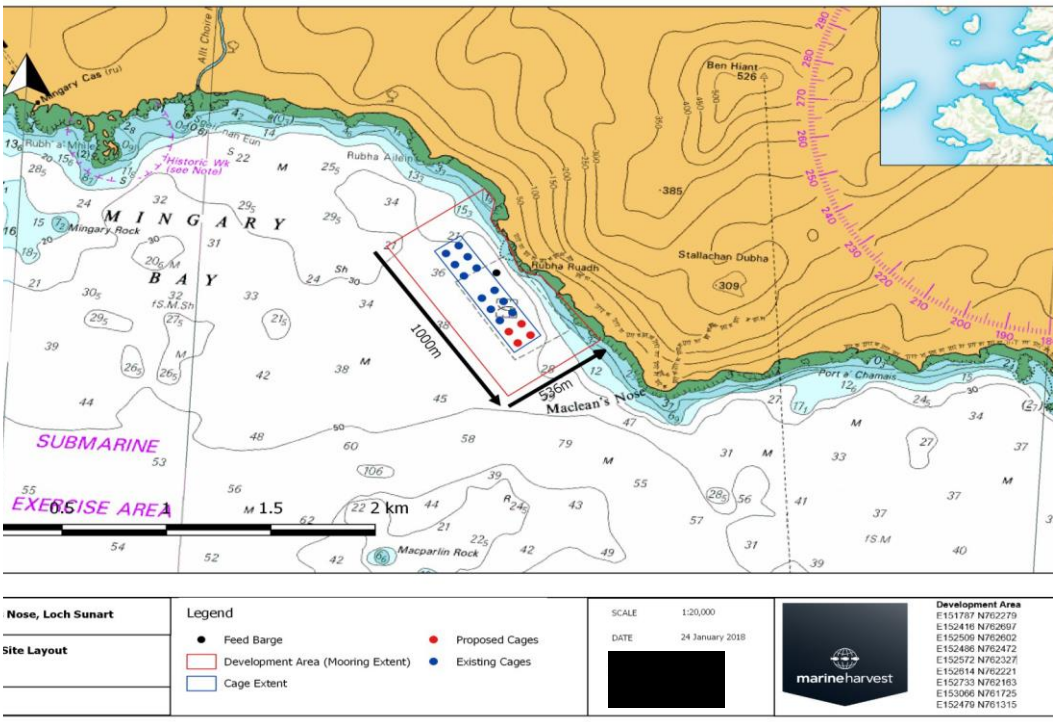

Figure 1. The proposed configuration of cages at Macleans Nose.

2.2 General Environmental Risks Associated with Aquaculture Discharges

The three main types of marine cage fish farm waste discharges comprise of solid waste, dissolved nutrient waste and medicinal treatments. The following summary of general risks is summarised from "Review of the Impacts of Salmon Farming in Scotland" (SAMS, 2018).

Solid Wastes

Solid waste comprises fish faeces and solid food that sink through the water column. Solid wastes can modify the chemistry, microbiology and ecological communities on the seafloor. The extent to which solid waste particles are dispersed by currents determines the area and intensities in which they accumulate on the seabed. In highly energetic areas, this material is likely to be dispersed and assimilated by the benthic fauna with little detectable accumulation or impact. However, in lower energy areas the sea bed may become enriched, changing the structure of the benthic fauna, and this is sometimes associated with sediment anoxia.

SEPA has adopted a variety of assessment techniques as part of its regulatory approach to match the scale of farmed-fish production to the environment's capacity to cope. Techniques are applied over different geographic areas depending on the specific fate and behaviour of pollutants. A defined suite of environmental standards is used to assess the impact of discharges from marine cage fish farms to ensure that natural flora and fauna and important habitats are not put at risk.

Dissolved Nutrients

Some components of uneaten food and faeces sink to the seabed, other parts will be suspended or dissolved and then transported within the water column. Carbon, nitrogen and phosphorus are the main nutrient components of discharged material, with nitrogen considered to have the greatest impact through its role as a limiting factor in phytoplankton growth and eutrophication. Increased concentrations of some of these nutrients can be observed close to farms, however this is not perceived to be a significant concern provided there is adequate dispersion.

Medicinal Discharges

Medicines are administered either by in-feed additives or through in situ bath treatments for topical treatments:

- Bath treatments require the enclosure of individual pens by a large tarpaulin, where the treatment is administered then discharged to the water column following completion.
- In-feed additives mixed into standard salmon feed pellets can sink through the water column onto the sea floor if uneaten or residues are discharged in salmon faeces. The main in-feed additive used to control sea lice is emamectin benzoate, an in-feed treatment used to control sea lice, considered to have potential impacts on crustaceans. The EQS approach now encompasses two separate standards across a near field and far field standard.

Site Specific Considerations

A number of protected sites and designated areas are relevant to the proposals at Maclean's Nose:

- Sunart SAC lies adjacent to the Maclean's Nose and is designated on the basis of a range of terrestrial and marine Qualifying Features including includes otters (*Lutra lutra*) and reefs.

- Maclean's Nose is located within the Loch Sunart to Sound of Jura MPA, designated on the basis of presence of Common skate (*Dipturus batis*), and geodiversity features (channels and troughs).
- Loch Sunart Nature Conservation Marine Protected Area (MPA): the site is located adjacent to the MPA, which supports a range of Priority Marine Features (PMFs) including aggregations of the rare organ pipe worm (*Serpula vermicularis*), northern feather star aggregations (*Leptometrica celtica*) and flame shells (*Limaria hians*).
- Sunart Special Site of Scientific Interest (SSSI)) is situated adjacent to Maclean's Nose and is notified for a range of marine species extending from the mean low tide water mark including egg wrack (*Ascophyllum nodosum*), rocky shores, eel grass beds and otters (*Lutra lutra*).

In addition, Maclean's Nose lies within 15 km of both the Ardnamurchan Burns SAC and Mingarry Burn SAC, both designated for freshwater pearl mussel (*Margaritifera margaritifera*) populations, however impacts from discharges are not anticipated to impact the qualifying features of these designations. Similarly, the Inner Hebrides and Minches candidate SAC, designated for Harbour porpoise populations, is also not predicted to be impacted by discharges arising from the development.

A baseline survey of benthos at Maclean's Nose was undertaken in 2013 where both video and sediment surveys were undertaken and reported. The biology of the seabed was described to consist of sparsely burrowed circalittoral fine mud with frequent observations of the tall seapen (*Funiculina quadrangularis*), the Phosphorescent seapen (*Pennatula phosphorea*) and an auger shell (*Turritella communis*). Infrequently the following were observed: tube anemone (*Cerianthus lloydii*), the Norwegian lobster (*Nephrops norvegicus*), a burrowing mud shrimp (*Callianassa subterranea*), a fireworks anemone (*Pachycerianthus multiplicatus)* and the hermit crab (*Pagurus bernhardus*). Overall, the habitat is classified as circalittoral fine mud with sea pens (SS.SMu.CfiMu.SpnMeg), the habitat quality of which is likely to be classed as medium to low; sea pen appearance is frequent, there is not a thick coverage and there is only one occurrence of a firework anemone and of one Norwegian lobster in the three transects, indicating that this is not an important area for either of these species.

Locational guidelines published by Marine Scotland Science designate semi-enclosed areas such as lochs and voes on the basis of predictive modelling techniques to estimate nutrient enhancement and benthic impacts. MacLean's Nose is located approximately 1km from the closest Locational Guidelines boundary at Loch Sunart in an open water site, and consequently is not categorised under the Locational Guidelines. A methodology to characterise the nutrient contribution based on calculation on the proposed nutrient budget, the Equilibrium Enhancement Contentration (ECE) and a Cumulative ECE assessment was undertaken and reported in the Environmental Impact Assessment Report. The nutrient contributions from Maclean's Nose represent 5.6% of background value, below the UKTAG trigger and are assessed as not significant. Similarly, the cumulative nitrogen contribution is assessed to contribute less than 1% of the background value and were assessed to be not significant.

Site Performance

The most recent compliance assessment report issued by SEPA in August 2017 indicated no breaches of Environmental Limit Conditions (ELC) and an overall interim Environmental Management Condition (EMC) assessment of 'High Performance', with the overall assessment indicating compliance. The previous Fish Farm Monitoring Report issued in July 2017 indicated that the cage edge station passed the benthic faunal criteria for within the Allowable

Zone of Effect (AZE), with sufficient abundances of polychaetes to rework the sediments. Other stations (AZE -10, AZE, and AZE+10) all passed benthic criteria overall.

3 HYDRODYNAMIC MODEL DESCRIPTION AND CONFIGURATION

3.1 Model Description

The water column in Loch Sunart is typically stratified and for this application, the Finite Volume Community Ocean Model (FVCOM) hydrodynamic model was used. FVCOM is a prognostic, unstructured-grid, finite-volume, free-surface, 3-D primitive equation coastal ocean circulation model developed by the University of Massachusetts School of Marine Science and the Woods Hole Oceanographic Institute (Chen et al., 2003). The model consists of momentum, continuity, temperature, salinity and density equations and is closed physically and mathematically using turbulence closure submodels. The horizontal grid is comprised of unstructured triangular cells and the irregular bottom is presented using generalized terrain-following coordinates. The General Ocean Turbulent Model (GOTM) developed by Burchard's research group in Germany (Burchard, 2002) has been added to FVCOM to provide optional vertical turbulent closure schemes. FVCOM is solved numerically by a second-order accurate discrete flux calculation in the integral form of the governing equations over an unstructured triangular grid. This approach combines the best features of finite-element methods (grid flexibility) and finite-difference methods (numerical efficiency and code simplicity) and provides a much better numerical representation of both local and global momentum, mass, salt, heat, and tracer conservation. The ability of FVCOM to accurately solve scalar conservation equations in addition to the topological flexibility provided by unstructured meshes and the simplicity of the coding structure has make FVCOM ideally suited for many coastal and interdisciplinary scientific applications.

FVCOM was originally developed for the estuarine flooding/drying process in estuaries and the tidal-, buoyancy- and wind-driven circulation in the coastal region featured with complex irregular geometry and steep bottom topography. This model has been upgraded to the spherical coordinate system for basin and global applications, although a cartesian grid was used here.

Configuration

The particle tracking model NewDepomod requires flow fields at relatively high spatial resolution, typically 25 m. This is higher than hydrodynamic models can feasibly be run over wide areas of the continental shelf (due to computational demands). It will be necessary therefore, to develop methods to provide high resolution flow fields over localised areas (e.g. 2km x 2km or larger) around sites. For the Macleans Nose site, a local area model of the Loch Sunart and western Sound of Mull (wSoM) region of the Inner Hebrides has been developed (Figure 2). This has a spatial resolution of typically 1 km at the outer boundaries, increasing to 20 m along the shoreline of Macleans Nose, and typically 25 – 30 m in the near-shore waters on the eastern Macleans Nose coast (Figure **3**).

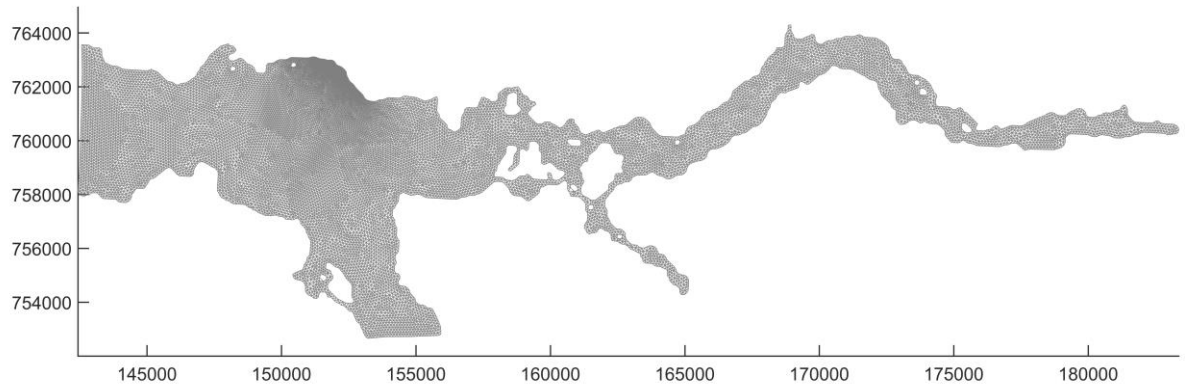

Figure 2. The unstructured mesh for the Loch Sunart/western Sound of Mull local area model.

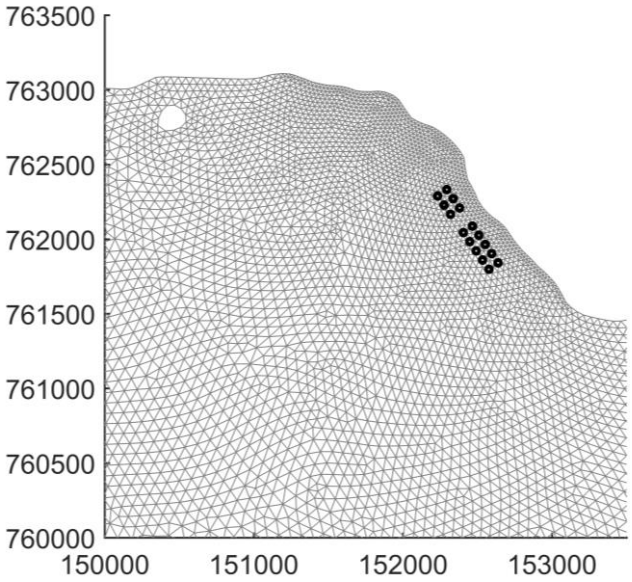

Figure 3. The unstructured mesh around the Macleans Nose site, with the proposed cage layout indicated (o).

The model uses a mesh of triangular elements. Equilateral triangular elements with a side length of 25 m have an area of ~540 m^2, slightly less than the cell area of a regular grid with 25 x 25 m cells, as commonly used within Depomod. In the Sunart/wSoM grid, the exact dimensions of individual triangles are variable, as the unstructured mesh grades from the areas of highest resolution (element side length ~20 m) around the farm site to those areas with lower resolution (Figure **3**). The Sunart/wSoM model has 15769 nodes and 29808 triangular elements.

The local area model was nested within the Wider Loch Linnhe System (WLLS) model, a sub-model of the Scottish Shelf Model (MSS, 2016a). The larger scale model is a fully baroclinic model, including tidal, meteorological and freshwater runoff forcing, and covers the south-

western Scottish shelf, from Ireland to Skye (Figure **4**). The WLLS output consists of a thirty-year climatology, with 'average' tides from 1993. From the year-long simulation of the WLLS model, the amplitudes and phases of eleven tidal constituents (MM, MF, O_1, K_1, Q_1, P_1, M_2, S_2, N_2, K_2, M_4) were extracted along the boundaries of the Sunart/wSoM model domain and used to force the latter model. The nesting process was one-way, and used only tidal elevation (not velocity) to force the Sunart/wSoM local area model.

Local bathymetry utilised all available sources. Bathymetry from the regional scale model was supplemented by local area bathymetry surveys, and other data sources e.g. the UKHO INSPIRE bathymetry data (http://aws2.caris.com/ukho/mapViewer/map.action). The latter included high-resolution bathymetry of a multi-beam survey of Loch Sunart conducted for SNH. These data were merged into a single dataset and used to provide water depths in the local area model (Figure 5 and Figure **6**).

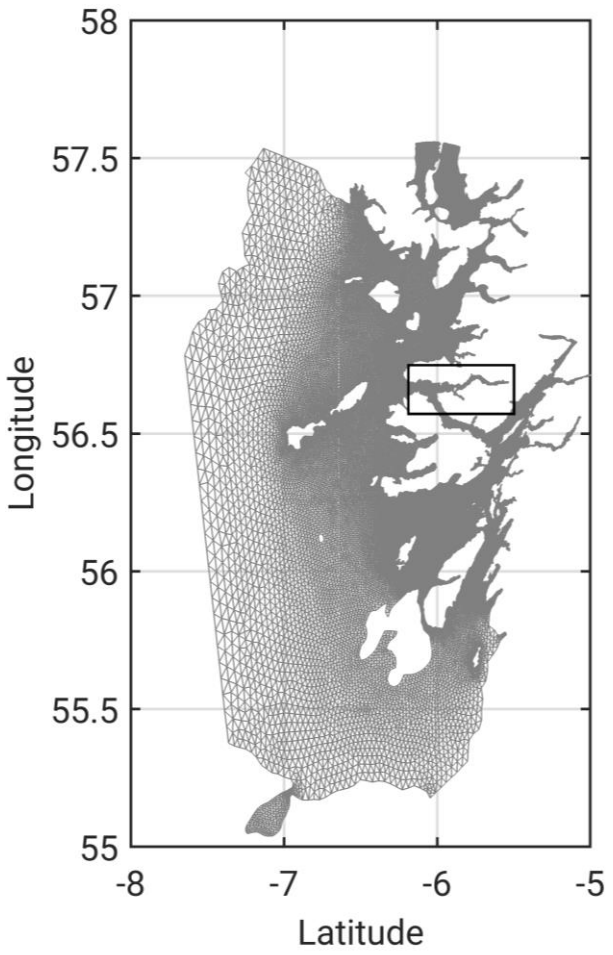

Figure 4. The WLLS model domain that provides boundary conditions for the Sunart/wSoM model (□)

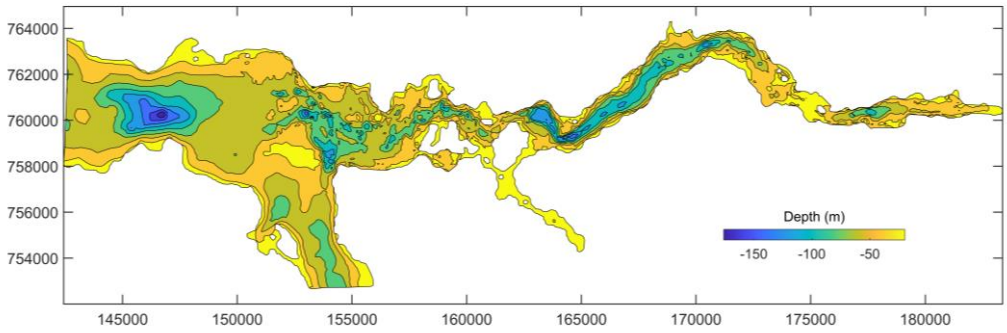

Figure 5. Water depths (m) in the Sunart/wSoM local area model.

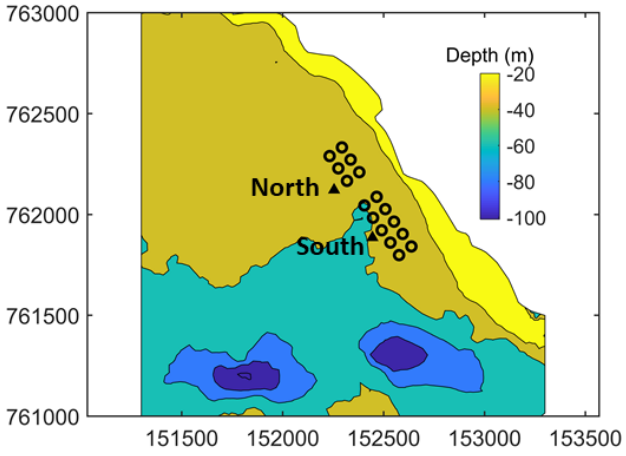

Figure 6. Water depths (m) in the Macleans Nose region. The locations of the north and south ADCP deployments (▲) and proposed cages (o) are shown.

Simulations were performed with and without wind forcing. When used, wind forcing was applied as a spatially-uniform wind stress calculated from hourly wind speed and direction data. Wind stress was calculated from the wind velocity by a standard quadratic relation

$$\tau_x = \rho_a C_D u W$$

$$\tau_y = \rho_a C_D v W$$

where (u,v) are the East and North components of wind velocity respectively, W is the wind speed ($W = [u^2+v^2]^{½}$), ρ_a is the density of air, and the drag coefficient C_D is calculated following Wu (1982).

River flow was taken from the 30-year Scottish Shelf Model climatology. Nine rivers enter the model domain shown in Figure 3, mostly small streams; the largest averaged input throughout the year is from the Carnoch River at the head of Loch Sunart (Figure 7). Thus the river flows used in the modelling here represent typical conditions rather than actual flows during the simulation periods.

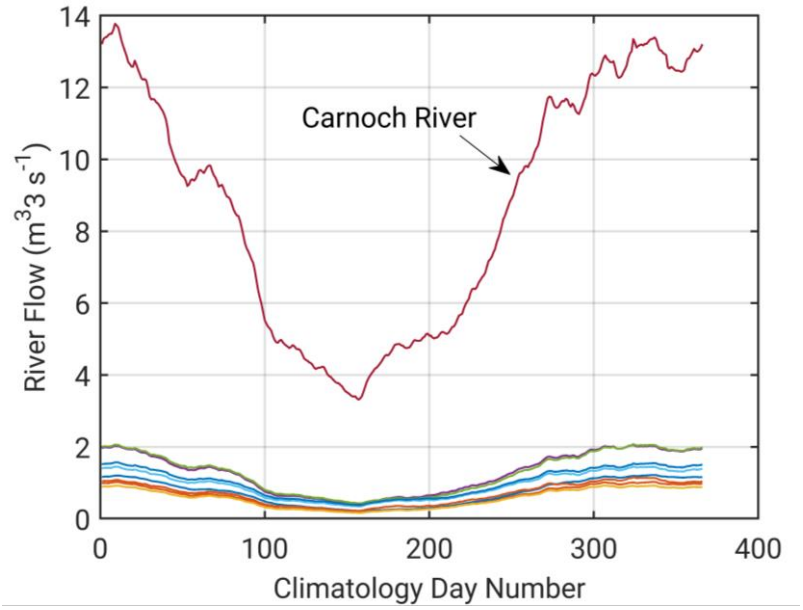

Figure 7. Averaged flows from 9 rivers and streams entering Loch Sunart and the western Sound of Mull from the 30-year climatology used by the Scottish Shelf Model. The largest flow is from the Carnoch River at the head of Loch Sunart.

The persistent stratification requires that the hydrodynamic model is run in three-dimensional mode. Here, we used 11 sigma levels, equally distributed through depth at σ = [0, -0.1, -0.2, -0.3, -0.4, -0.5, -0.6, -0.7, -0.8, -0.9, -1.0]. Velocities in FVCOM are calculated mid-layer, hence the velocity closest to the bed was calculated at σ = -0.95.

3.2 Calibration

The local area model was calibrated against current data and seabed pressure data, measured in the local Macleans Nose area using Acoustic Doppler Current Profilers (ADCP). Data are available from:

(i) 22nd March – 4th May 2017
(ii) 5th May – 3rd July 2017

In total, the data extend over 102 days. Two ADCPs were deployed on both occasions (Figure 6) and were both used for the calibration/validation. Calibration was performed in a standard fashion, with bed friction and diffusion/dispersion coefficients adjusted to obtain the best fit against the observed sea surface height and current data. For the present location, stratification was considered to be significant and the model was run in 3D mode. The model was run for the same period as the observations and the modelled tidal elevation and velocity at the site evaluated against the observed data. Observed tidal elevations and velocities were extracted from the observational data using t-tide (Pawlowicz et al., 2002). Boundary temperature and salinity, and river flow data, were taken from the 30-year climatology

produced by the Scottish Shelf Model (MSS, 2016b), corresponding to the time of year of the observations (March – July). The calibrated modelled elevation and velocity are presented alongside the observed data below.

The model was run with and without local wind forcing applied to the local area model. Hourly wind speed and direction data from the Met Office meteorological station at Tiree were used.

4. HYDRODYNAMIC MODELLING RESULTS

4.1 Calibration, May – July 2017

The calibration used observed depth and current velocity from the ADCP location to compare with modelled sea surface height (SSH) and velocity. The calibration focussed on the tidal SSH and velocity only. Because the wind forcing used was spatially non-varying, it is unlikely that the resulting non-tidal flow fields will accurately represent the observed non-tidal flow data; what we intend is that by applying some wind forcing, an appropriate level of additional energy will be applied to the system. For calibration purposes, the tidal currents should be a more reliable means of calibrating the model.

The model was calibrated by varying the value of the bed roughness lengthscale, z_0, which determines the frictional effect of the seabed on the flow, and the horizontal and vertical viscosity parameters. Simulations were performed with a range of values of z_0, varying over two orders of magnitude, $0.001 \leq z_0 \leq 0.1$ m. A Smagorinsky scheme was used for the horizontal diffusion and viscosity, and a Mellor-Yamada Level 2.5 turbulence closure sub-model for the vertical diffusivity and viscosity. After numerous simulations, a final parameter set was selected (Table 1).

Table 1. Parameter values chosen for the FVCOM model during the calibration simulations.

Parameter Description	Value
Bed roughness lengthscale, z_0 (m)	0.01
Smagorinsky coefficient	0.2
Background viscosity ($m^2\ s^{-1}$)	10^{-5}
Background diffusivity ($m^2\ s^{-1}$)	10^{-6}

The results of the calibration exercise are presented in Figure 8, Figure 9 and Table 2 - Table 4. The sea surface height was reasonably accurately modelled, with model skill of 0.97 at both locations. The MAE and RMSE values of 0.34 m and 0.41 m respectively are about 7.5% and 9% of the spring tide range respectively. The model under-predicted the tidal range during alternate spring tides e.g. in mid-April 2017 and slightly over-predicted the range during neaps (Figure 8). The observed and modelled time series of SSH at the south site, which are not shown, were almost identical.

North and east components of velocity at the north ADCP location were satisfactorily reproduced by the model, with values of d_2 exceeding 0.6 at all depths, except for the north component at the surface where d_2 = 0.59 (Table 3). Here, the model under-predicted the magnitude of the observed northward component (Figure **9**). At the mid-depth and near-bed depths, the magnitude of the modelled current closely matched that of the observed currents. Values of MAE and RMSE were typically 1 – 3 cm s^{-1} (Table 3).

At the southern ADCP location, the model also largely reproduced the observed magnitude of the observed currents. The exception again, was the surface northward component, which the model under-predicted quite significantly. The values of model skill, d_2, again exceeded 0.6, except for the near-bed eastward velocity (Figure **13**); at this location and depth, however, the current was predominantly north-south, and the eastward component was weak, increasing the error as a proportion of the velocity. Values of the MAE and RMSE at the south location were typically 2 – 3 cm s-1 (Table 4).

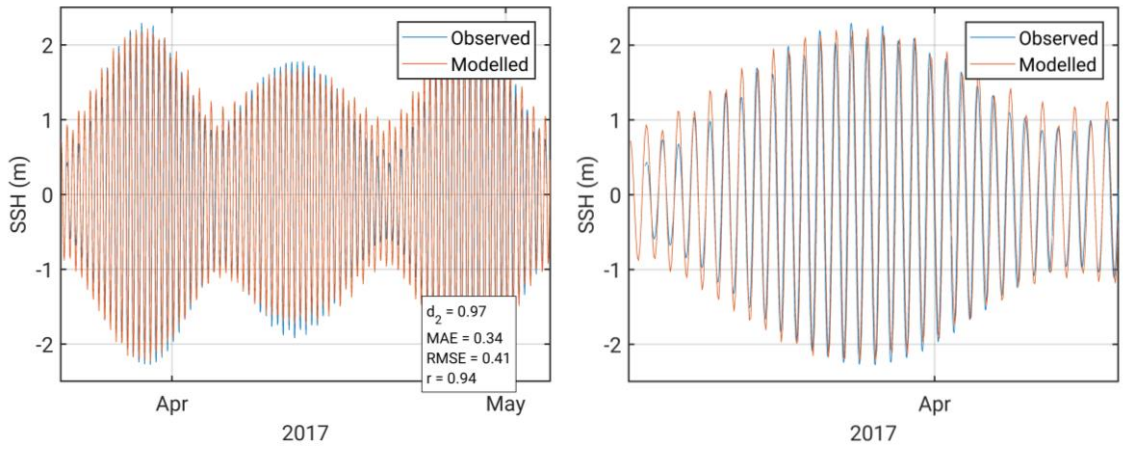

Figure 8. Comparison between observed and modelled sea surface height at the northern ADCP location from March - May 2017 with parameter values from Table 1. Both the full record (left) and a subset of 15 days (right) are shown. Observed data are in blue, modelled data in red.

Our focus during the calibration exercise was to simulate the near-bed currents as accurately as possible, since the near-bed currents have most influence on the benthic footprint and emamectin benzoate residue distributions. Macleans Nose is a challenging location to model, situated at the confluence of Loch Sunart and the Sound of Mull. Internal tides are known to propagate in Loch Sunart (Elliott et al., 1992) and the current data obtained at Macleans Nose provides evidence that internal waves were propagating past the site (a mid-depth phase shift of 180° in the M_2 constituent). This makes accurate simulation more difficult, as the current flows depend on the exact structure of water column stratification at the time of the observations. Our focus was to simulate currents, particularly near-bed currents, with the same magnitude and direction as the observed data, even if the temporal variability of the modelled currents did not match the observed variability exactly.

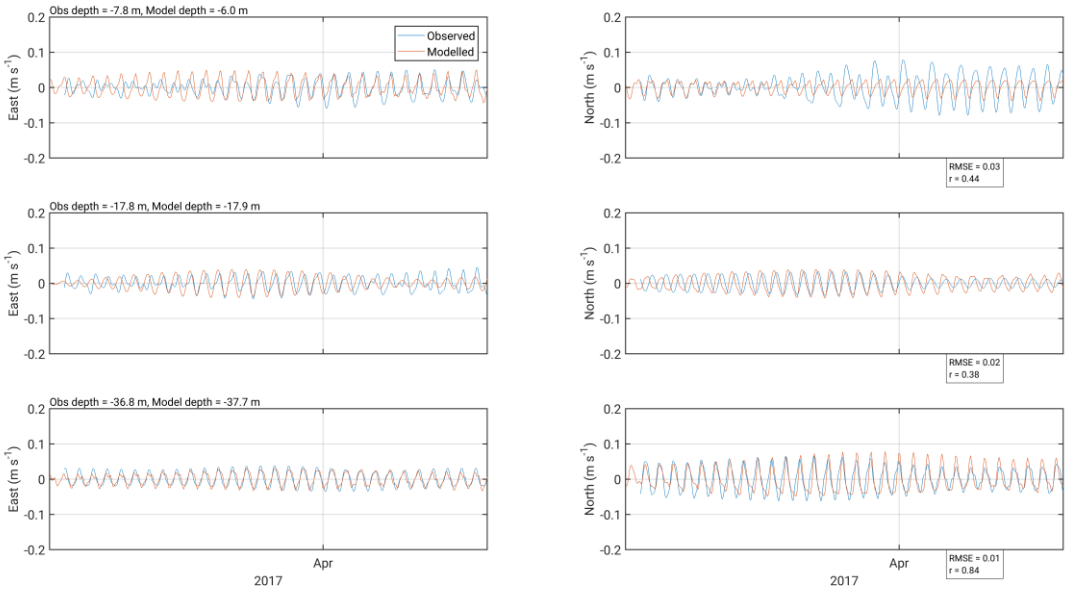

Figure 9. Comparison between observed and modelled East (left) and North (right) components of near-surface (top), mid-depth (middle) and near-bed (bottom) velocity at the northern ADCP location in March – May 2017. Observed data are in blue, modelled data in red.

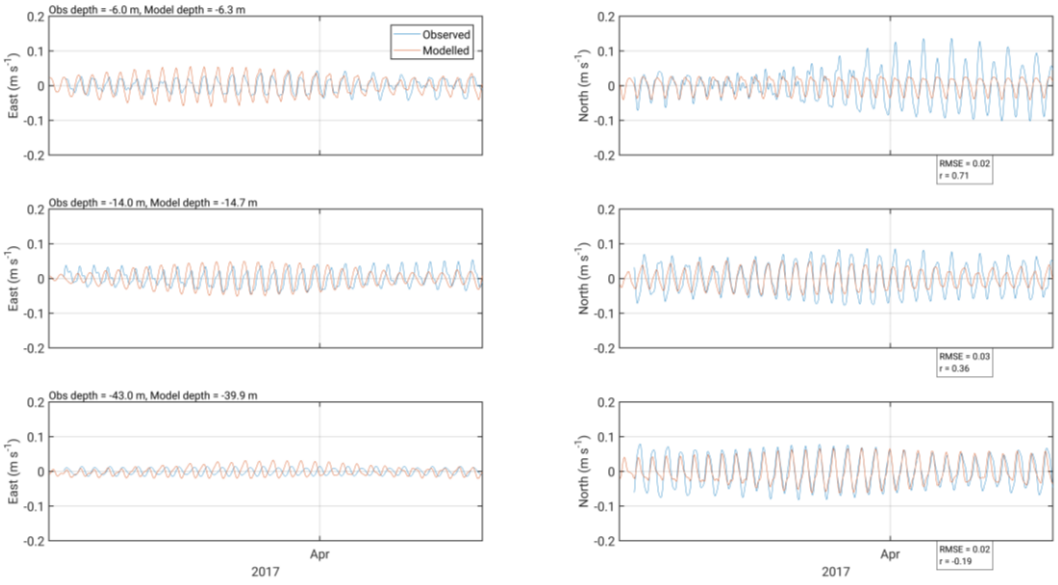

Figure 10. Comparison between observed and modelled East (left) and North (right) components of near-surface (top), mid-depth (middle) and near-bed (bottom) velocity at the southern ADCP location in March – May 2017. Observed data are in blue, modelled data in red.

Table 2. Model performance statistics for sea surface height (SSH) at the north and south ADCP locations from the selected calibration simulation, March – May 2017.

	North	South
Skill, d_2	0.97	0.97
Mean Absolute Error (MAE)	0.34 m	0.34 m
Root-Mean-Square Error (RMSE)	0.41 m	0.41 m

Table 3. Model performance statistics for east and north components of velocity at the north ADCP location from the selected calibration simulation, March – May 2017.

	ADCP Depth (bin)	Model Depth	Metric	East	North
Surface	7.8 m (30)	6.0	d_2	0.66	0.59
			MAE	0.02	0.02
			RMSE	0.03	0.02
Middle	17.8 m (20)	17.9	d_2	0.64	0.63
			MAE	0.02	0.02
			RMSE	0.02	0.02
Bottom	36.8 m (1)	37.7	d_2	0.91	0.89
			MAE	0.01	0.02
			RMSE	0.01	0.02

Table 4. Model performance statistics for east and north components of velocity at the south ADCP location from the selected calibration simulation, March – May 2017.

	ADCP Depth (bin)	Model Depth	Metric	East	North
Surface	6.0 m (38)	6.3	d_2	0.81	0.69
			MAE	0.02	0.03
			RMSE	0.02	0.04
Middle	14.0 m (30)	14.7	d_2	0.62	0.77
			MAE	0.02	0.03
			RMSE	0.03	0.03
Bottom	43.0 m (1)	39.9	d_2	0.26	0.89
			MAE	0.01	0.02
			RMSE	0.02	0.03

Histograms of the measured and modelled current speed and direction demonstrate that the model captures the main features of the observed flow (Figure **11**). The distributions of current speed at mid-depth and near-bed closely resembled the observed distribution, and the modelled direction is essentially north-south near the bed and north-northwest to south-southeast at mid-depth, as observed. At the near-surface depth, the modelled currents are weaker than the observed; this may be a result of the internal wave activity, but since near-surface currents do not strongly affect particulate deposition, the weaker modelled flows are not of great concern. The direction of the modelled near-surface flows is also more variable than observed (Figure **11**).

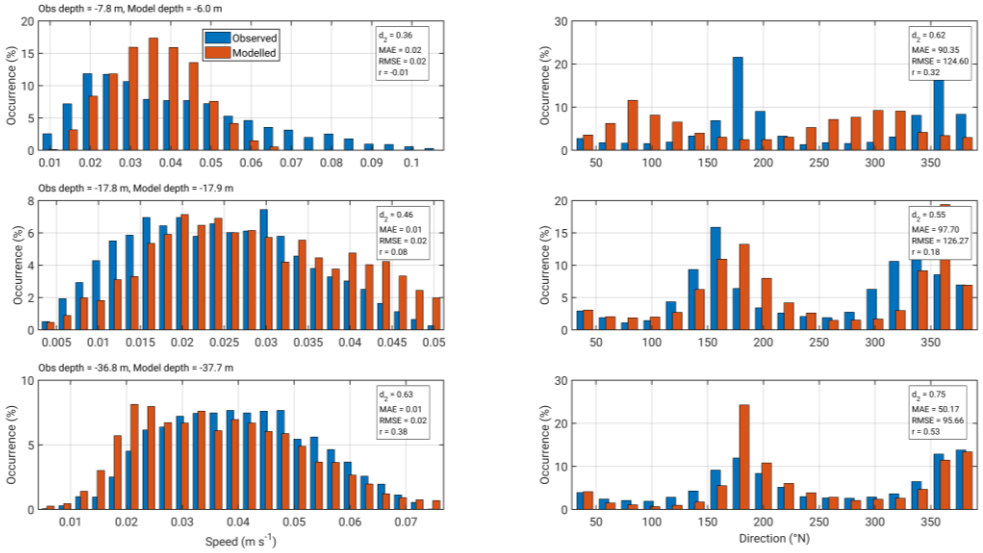

Figure 11. Histograms of measured and modelled current speed (left) and direction (right) at near-surface (top), mid-depth (middle) and near-bed (bottom) depths for the north ADCP location during March – May 2017.

At the south location, the model did not capture the highest current speeds (Figure **12**), with a high frequency of predicted currents in the range of 3 – 5 cm s^{-1}. This under-prediction was evident at all three depths, and makes the model slightly conservative in terms of dispersive energy at this location. Modelled current direction broadly matched the observed direction at mid-depth and near the bed; at the surface, the modelled direction was uniformly distributed, not strongly capturing the strongest flows to the south. Again, however, the surface currents have a negligible effect on particulate waste dispersion, and this shortcoming in the model performance is not considered critical.

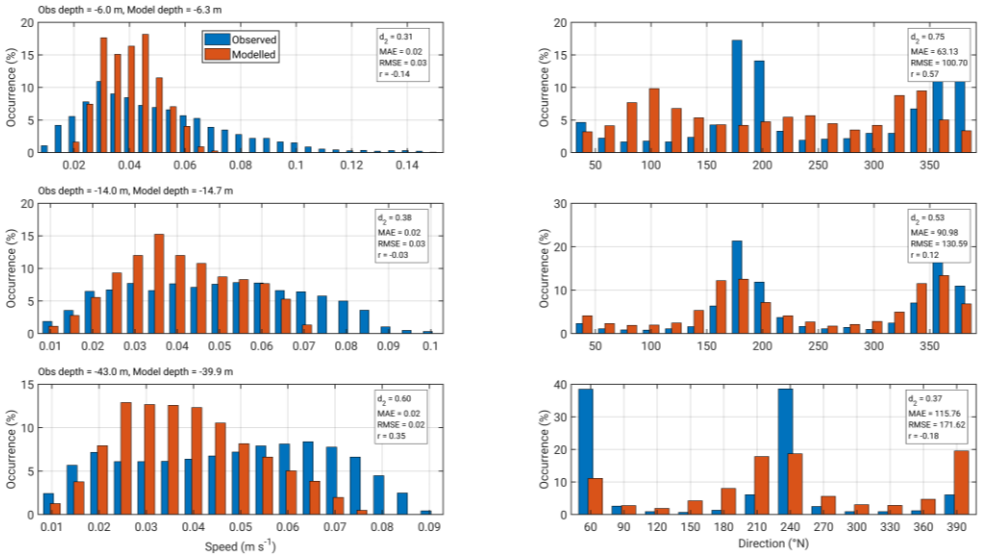

Figure 12. Histograms of measured and modelled current speed (left) and direction (right) at near-surface (top), mid-depth (middle) and near-bed (bottom) depths for the south ADCP location during March – May 2017.

4.2 Validation, April – May 2010

The model was validated against ADCP data from two locations from May – July 2017 (Figure **6**). The validation looks first at sea surface height, as measured by the ADCP pressure sensors, and secondly at the north and east components of velocity.

4.2.1 Sea Surface Height

Observed and modelled sea surface height (SSH) from May – July 2017 are shown for Macleans Nose North (Figure **13**) and Macleans Nose South (Figure **14**). As for March – May 2017, the agreement between model and data is reasonable at both sites, with a model skill d_2 exceeding 0.95 (Table 5). The MA and RMS errors are of similar magnitude as the calibration errors, about 7.5 – 9% of the spring tidal range.

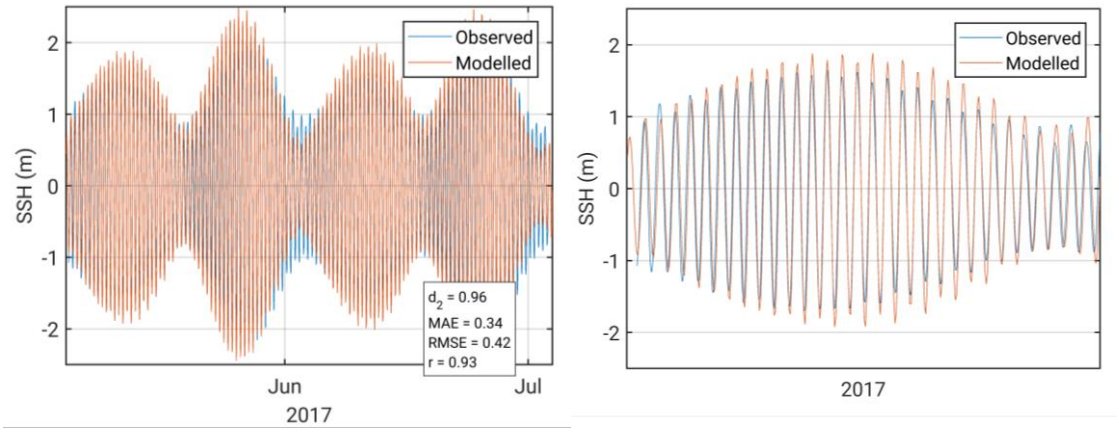

Figure 13. Comparison between observed and modelled sea surface height at the northern ADCP location from May – July 2017 with parameter values from Table 1. Both the full record (left) and a subset of 15 days (right) are shown. Observed data are in blue, modelled data in red.

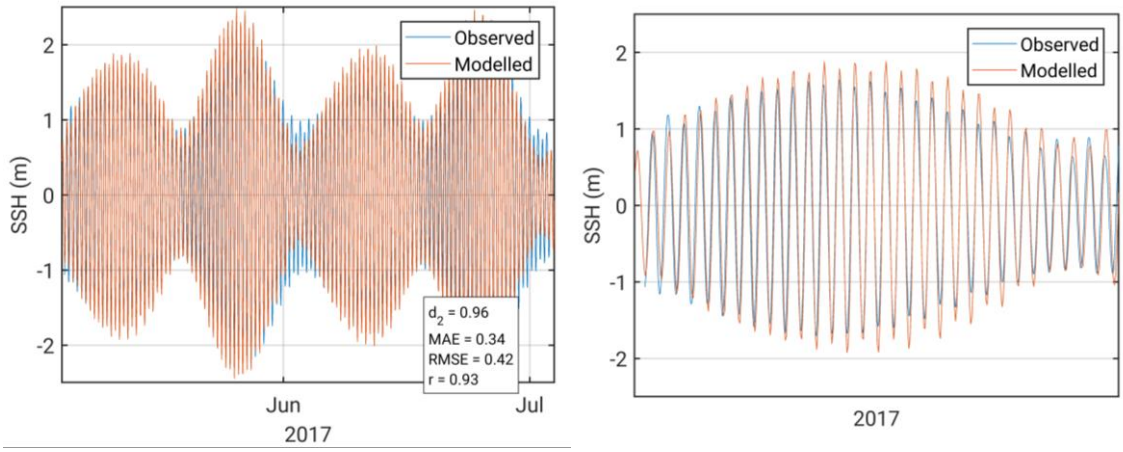

Figure 14. Comparison between observed and modelled sea surface height at the southern ADCP location from May – July 2017 with parameter values from Table 1. Both the full record (left) and a subset of 15 days (right) are shown. Observed data are in blue, modelled data in red.

Table 5. Model performance statistics for sea surface height (SSH) at the north and south ADCP locations from the validation simulation, May – July 2017.

	North	**South**
Skill, d_2	0.96	0.96
Mean Absolute Error (MAE)	0.34	0.34
Root-Mean-Square Error (RMSE)	0.42	0.42

4.2.2 Velocity Time Series

Results from the validation exercise for the velocity are presented in Figure **15** and Figure **16**. The currents at the site have a stronger north-south component, particularly near the seabed. The model correctly reproduced the difference in relative magnitude between the components of velocity at both North and South sites. However, the modelled phases were less accurately modelled at the surface and mid-depth; this is thought to be due to internal wave activity which modifies the phase of the observed currents. Although the phase of the flow was not quite captured by the model, the magnitude of the current speed was similar to the observed speed. This is important for the settling and erosion of sediments which is a function of near-bed current speed and stress.

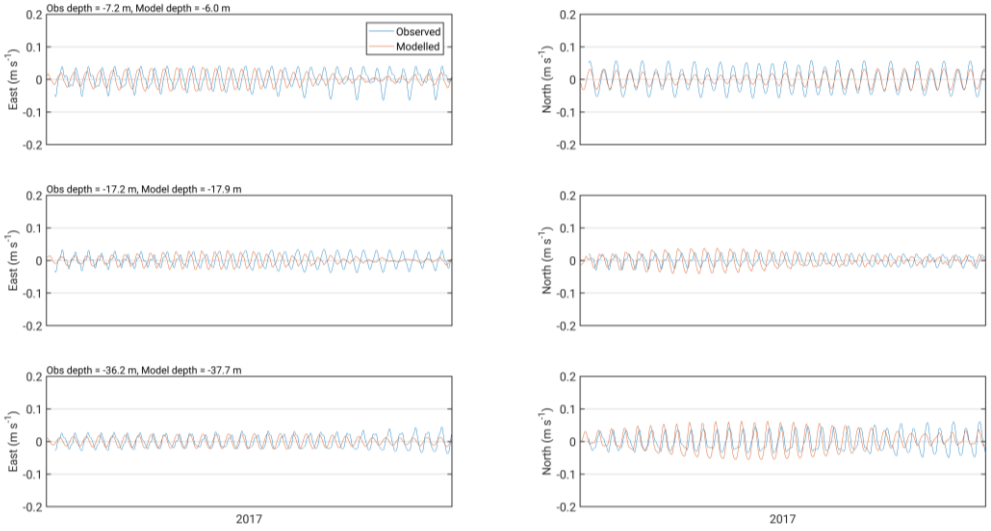

Figure 15. Comparison between observed and modelled East (left) and North (right) components of near-surface (top), mid-depth (middle) and near-bed (bottom) velocity at the northern ADCP location in May – July 2017. Observed data are in blue, modelled data in red.

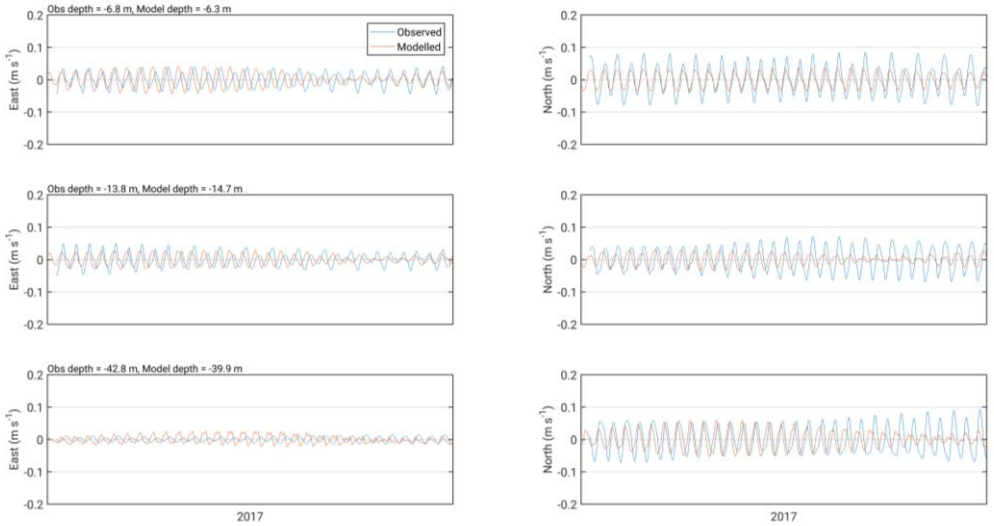

Figure 16. Comparison between observed and modelled East (left) and North (right) components of near-surface (top), mid-depth (middle) and near-bed (bottom) velocity at the southern ADCP location in May – July 2017. Observed data are in blue, modelled data in red.

Table 6. Model performance statistics for east and north components of velocity at the north ADCP location from the validation simulation, May – July 2017.

	ADCP Depth (bin)	Model Depth	Metric	East	North
Surface	7.2 m (30)	6.0	d_2	0.52	0.87
			MAE	0.02	0.02
			RMSE	0.03	0.02
Middle	17.2 m (20)	17.9	d_2	0.55	0.45
			MAE	0.02	0.02
			RMSE	0.02	0.02
Bottom	36.2 m (1)	37.7	d_2	0.77	0.83
			MAE	0.01	0.02
			RMSE	0.02	0.02

Table 7. Model performance statistics for east and north components of velocity at the south ADCP location from the validation simulation, May – July 2017.

	ADCP Depth (bin)	Model Depth	Metric	East	North
Surface	6.8 m (37)	6.3	d_2	0.63	0.83
			MAE	0.02	0.02
			RMSE	0.02	0.03
Middle	13.8 m (30)	14.7	d_2	0.61	0.59
			MAE	0.02	0.03
			RMSE	0.02	0.03
Bottom	42.8 m (1)	39.9	d_2	0.38	0.75
			MAE	0.01	0.03
			RMSE	0.01	0.03

Histograms of the velocity at the north and south sites demonstrate that the model broadly captures the orientation and magnitude of the observed flow (Figure 17 and Figure 18). The modelled flows underestimate the maximum observed speeds, particularly at the near-surface depth at both sites and rather more at the southern location than the northern location. The orientation of the modelled flow broadly resembles the observed orientation, particularly for at the mid-depth and near-bed depths.

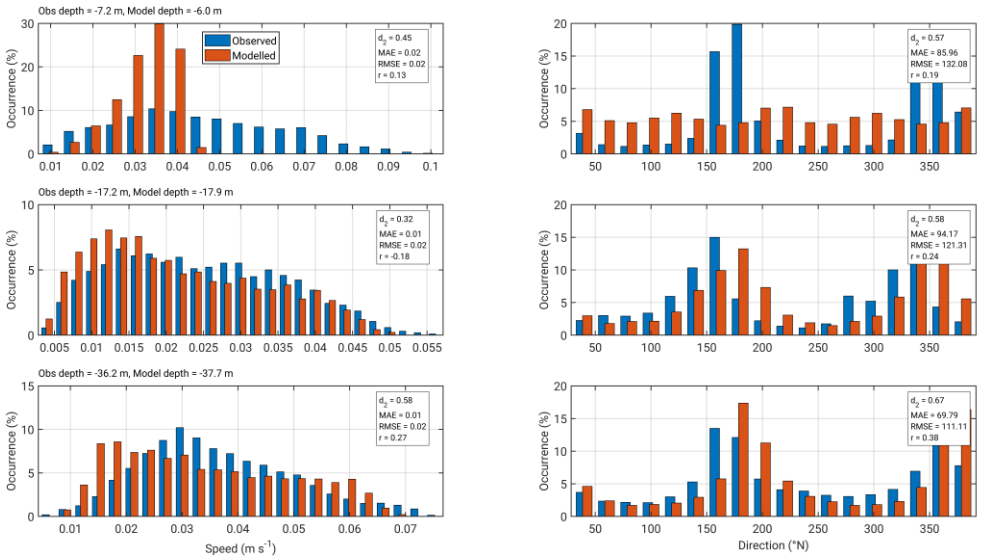

Figure 17. Histograms of measured and modelled current speed (left) and direction (right) at near-surface (top), mid-depth (middle) and near-bed (bottom) depths for the north ADCP location during May – July 2017.

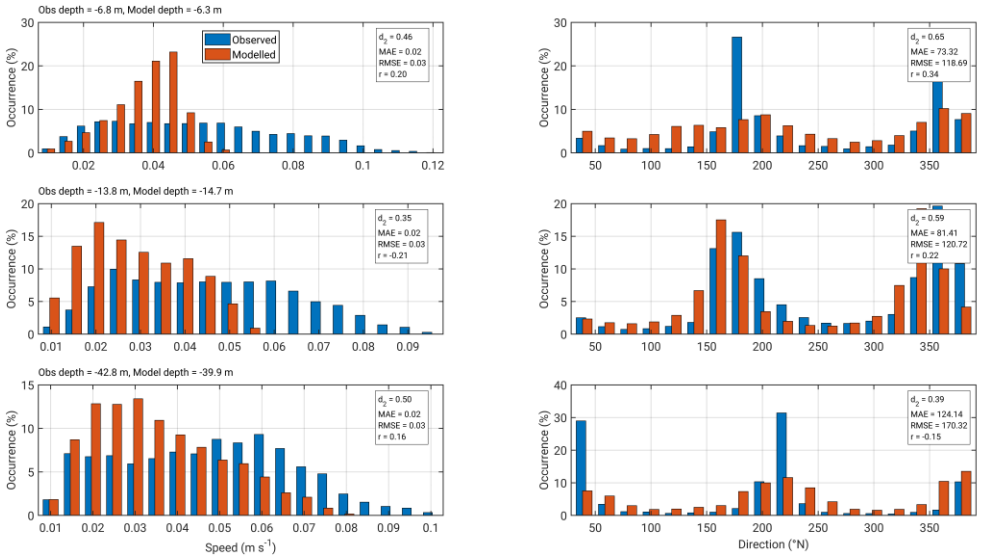

Figure 18. Histograms of measured and modelled current speed (left) and direction (right) at near-surface (top), mid-depth (middle) and near-bed (bottom) depths for the south ADCP location during May – July 2017.

Overall, the calibration and validation exercise indicates that the model broadly reproduces the observed sea surface height and velocity data, particularly the near-bed velocity which is important for the particulate waste modelling using NewDepomod. The modelled velocity under-predicted the observed data, particularly at the southern location, but this can be considered to provide a degree of conservatism to the predictions of waste dispersion by NewDepomod.

4.3 Modelled Flow Fields

Modelled flood and ebb vectors at spring tides are illustrated in Figure 19 and Figure 20. To the east of Macleans Nose, in the vicinity of the farm site, flood currents are typically northward, veering between north-northwest and north-northeast. Ebb tide currents are toward the south-southeast, parallel to the east Macleans Nose coastline.

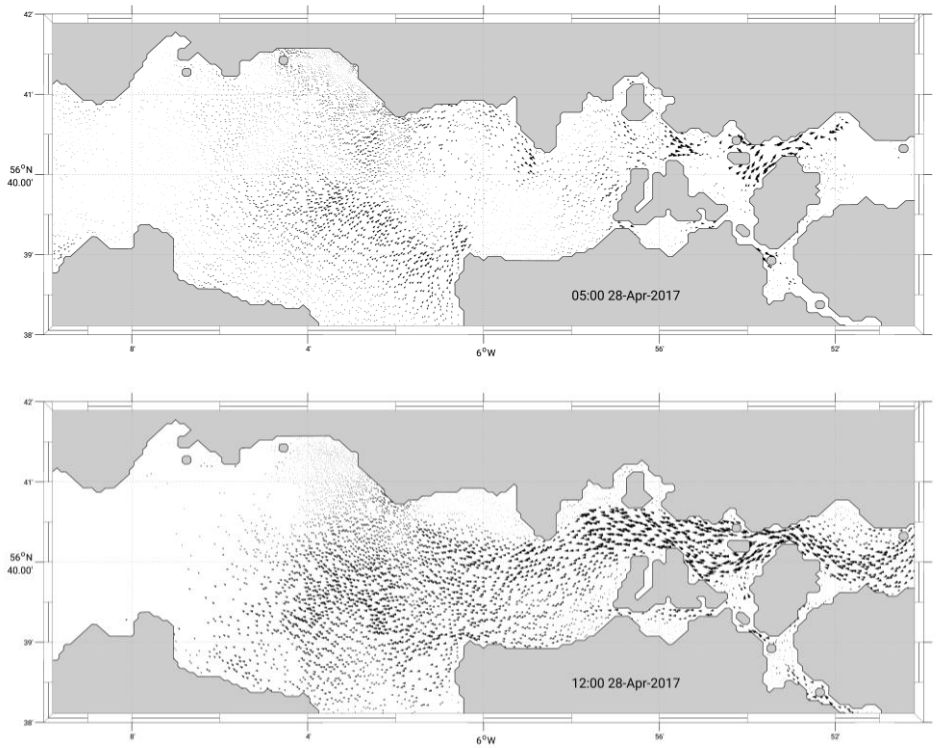

Figure 19. Modelled surface flood (top) and ebb (bottom) tide current vectors at spring tide on 28th April 2017. Every third vector is shown.

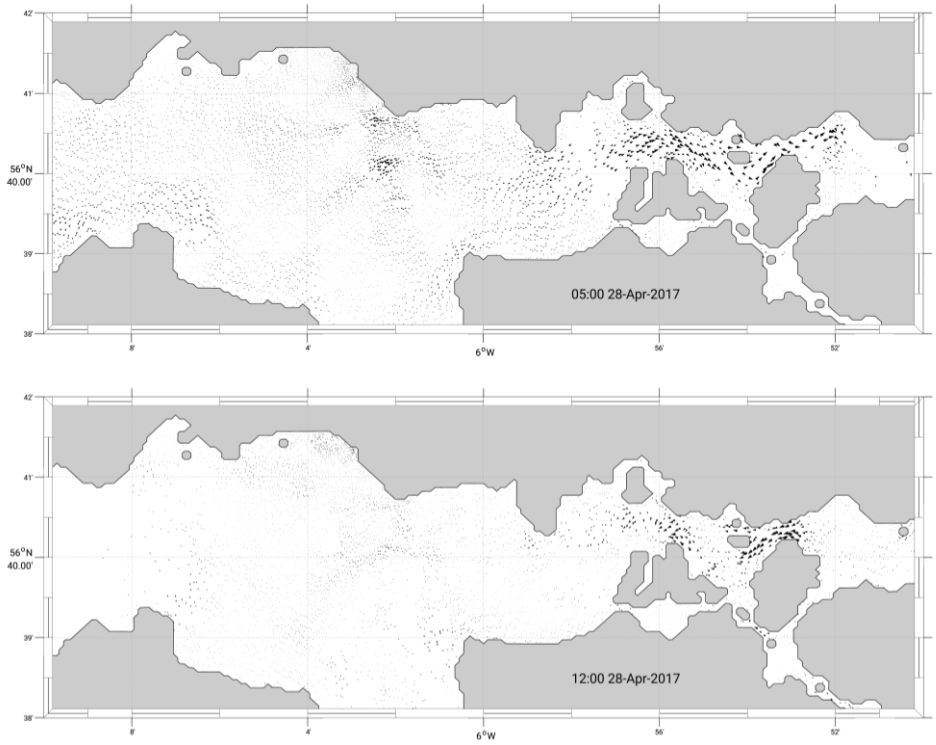

Figure 20. Modelled near-bed flood (top) and ebb (bottom) tide current vectors at spring tide on 28th April 2017. Every third vector is shown.

4.4 Preparing Velocity Data for NewDepomod

The particle tracking model NewDepomod requires flow fields at relatively high spatial resolution, typically 25 m. In order to provide a relatively uniform distribution of velocity data at grid nodes, an unstructured grid of the local area was developed (Figure 21), using the Blue Kenue software (https://www.nrc-cnrc.gc.ca/eng/solutions/advisory/blue_kenue_index.html). For the grid here, the number of nodes was 2799, with 5357 triangular elements. Grid resolution varied smoothly, from about 35m around the edge of the grid to ~20 m at the Macleans Nose coastline. The mean element area was 564 m^2.

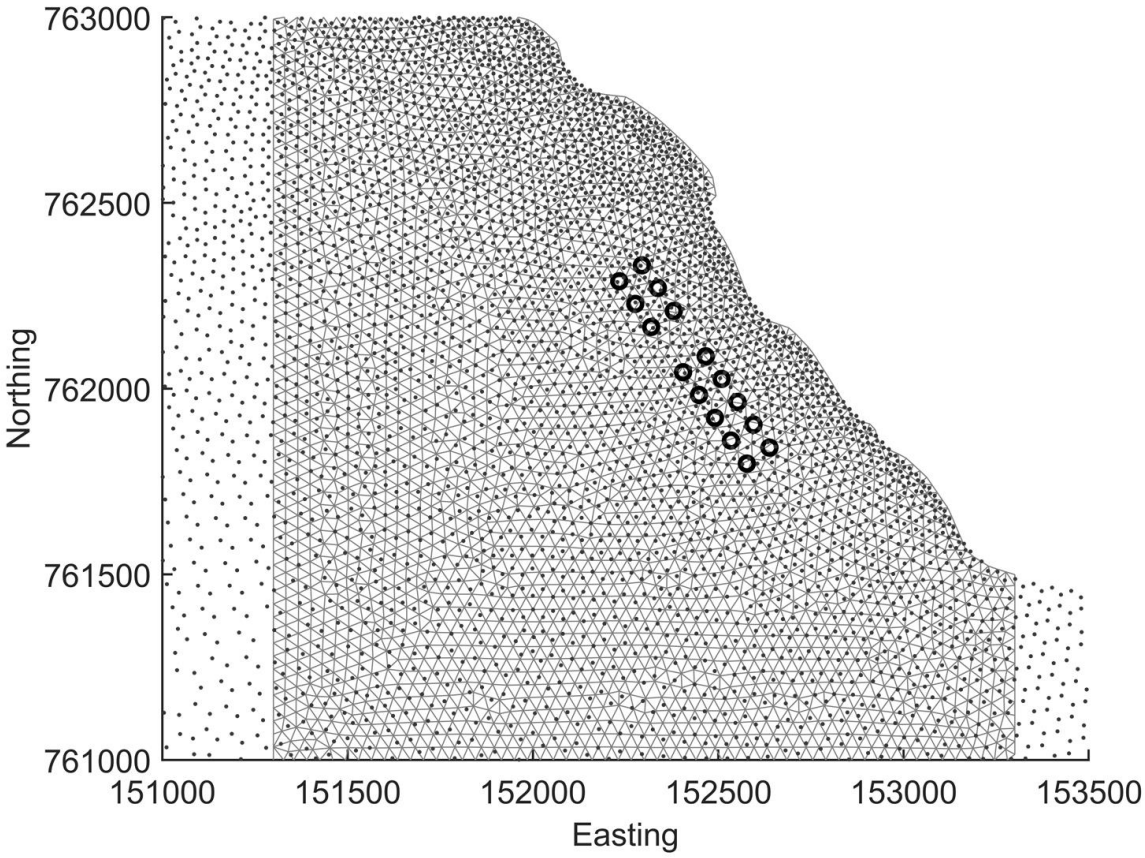

Figure 21. The NewDepomod unstructured mesh for Macleans Nose, with the proposed cage locations (**o**) and the locations of the FVCOM hydrodynamic model cell centres (·) indicated.

Velocities at the NewDepomod grid nodes were interpolated from the cell centres of the hydrodynamic model described above. The flow around the Macleans Nose site was highly resolved in the hydrodynamic model (Figure 21). The interpolation from the HD grid to the NewDepomod grid was performed in Matlab, using the 'natural' scattered interpolant routine. Velocity data from the HD model were provided to NewDepomod at three depths, corresponding to sigma layers at σ = [-0.00, -0.55, -0.95]. Velocity data at a fourth level, σ = -

1.0, are also provided as standard, with u = v = 0.0. The simulations used for the NewDepomod modelling are described below.

5. NEWDEPOMOD MODELLING

5.1 Initial Testing

Initial testing of NewDepomod was undertaken by running the Brickman test (Brickman et al., 2009). This standard test assesses the ability of particle tracking models to accurately simulate advection in spatially-varying flow fields. In this instance, the tests, which were successful, provided confidence that NewDepomod was correctly reading and utilising the spatially-varying flow fields from the hydrodynamic model. The tests also confirmed the initial settling phase of particles. The tests are not described further here, but the results are available at Marine Harvest.

5.2 Calibration and Validation Simulations

Calibration simulations, comparing predicted results against observed benthic and Slice residue data, were first undertaken. Slice was used at Macleans Nose in 2015, 2016 and 2017 (Table 8) with residue surveys taking place in February 2016, and May and October 2017, with the largest number of samples being collected during May 2017. At the same times, benthic surveys were also undertaken. Based on this data collection, six calibration/validation simulations were performed:

Calibration:

(i) Slice ("EmBZ"), 3rd October 2016 – 5th May 2017 (214 days)
(ii) Benthic ("NONE"), 3rd October 2016 – 5th May 2017 (214 days)

Validation:

(iii) Slice ("EmBZ"), 17th July 2015 – 12th February 2016 (210 days)
(iv) Slice ("EmBZ"), 3rd October 2016 – 24th October 2017 (386 days)
(v) Benthic ("NONE"), 17th July 2015 – 12th February 2016 (210 days)
(vi) Benthic ("NONE"), 3rd October 2016 – 24th October 2017 (386 days)

The start dates of these simulations corresponded to site stocking (see below for further comment on the duration of the simulations). The end dates corresponded with the Slice residue/seabed surveys.

During the calibration simulations (i) and (ii), parameter settings in NewDepomod were varied widely to achieve the best agreement between the model results and the observed data from the compliance and residue sampling (see below).

Flow fields were generated using the hydrodynamic model for the periods above. Given memory limitations of NewDepomod, the flow files were limited in size to about 100 days, whereas the simulations above ran for more than 200 days. The flow files therefore covered shorter periods than the NewDepomod simulations and flow fields repeated during the simulations. Typically, the hydrodynamic model was run for the later stages of the NewDepomod simulation period, to best approximate conditions at the times of the residue and seabed surveys. Two hydrodynamic model simulations were used for runs (i) to (vi) above, covering the periods:

a. 18th January – 5th May 2017 (107 days)
b. 30th October 2015 – 12th February 2016 (105 days)

The NewDepomod and HD model runs were designed to ensure that the flow fields were applied at the correct times during the later stages of the simulation, prior to the compliance surveys. The lengths of the NewDepomod simulations were therefore exactly an integer multiple of the length of the corresponding hydrodynamic model simulation. The longest Depomod simulations (iv and vi) used HD model output from Run a: January – May 2017.

Table 8. Slice (active ingredient: emamectin benzoate, "EmBZ") treatments and residue surveys during the 2015-16 and 2016-17 production cycles at Macleans Nose.

Cycle	Treatment start	Treatment End	EmBZ Mass (kg)	Survey Date
2015 – 16	01 Sept 2015	07 Sept 2015	0.384	11 Feb 2016
2016 – 17	30 Oct 2016	4 Nov 2016	0.056	03 – 04 May 2017
2016 - 17	29 Apr 2017	5 May 2017	0.358	24 Oct 2017

For the 2016-17 calibration, the hydrodynamic model was run for 107 days (18th January – 5th May 2017) and the NewDepomod simulation for 214 days (3rd October 2016 – 5th May 2017). For 2015-16, the hydrodynamic model and NewDepomod simulations ran for 105 and 210 days respectively.

5.3 Model Inputs and Flow Fields

5.3.1 Wind Forcing

In addition to the tide-only simulations, the model was run with wind forcing applied to give "Full Flow" velocity fields. Wind speed and direction data were obtained from the UK Meteorological Office Land Station on Tiree. For the period October 2015 – February 2015, only data with wind speeds greater than 9 m s^{-1} were obtained (Figure 22). For January – May 2017, a full record of hourly wind speed and direction was obtained (Figure 23). The wind

forcing was applied uniformly across the whole model domain (Figure 2). For the 2015 simulation, the patchy data were interpolated to hourly data using a cubic spline.

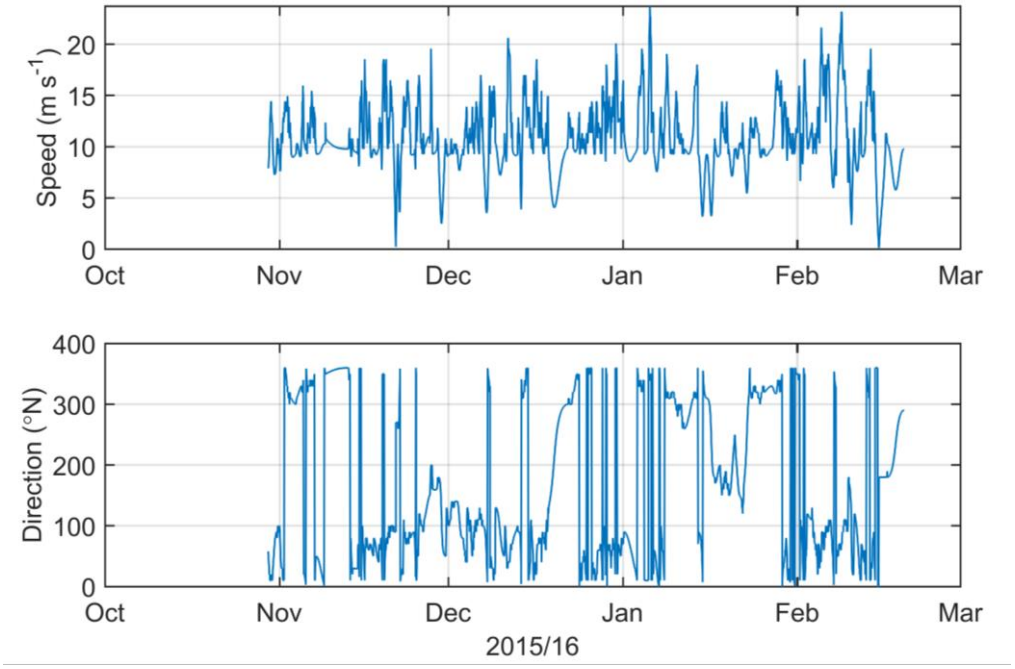

Figure 22. Hourly measured wind speed and direction from Tiree for the period 30th October 2015 – 12th February 2016. Data were only obtained for wind speeds exceeding 9 m s^{-1}. The direction data are in meteorological convention.

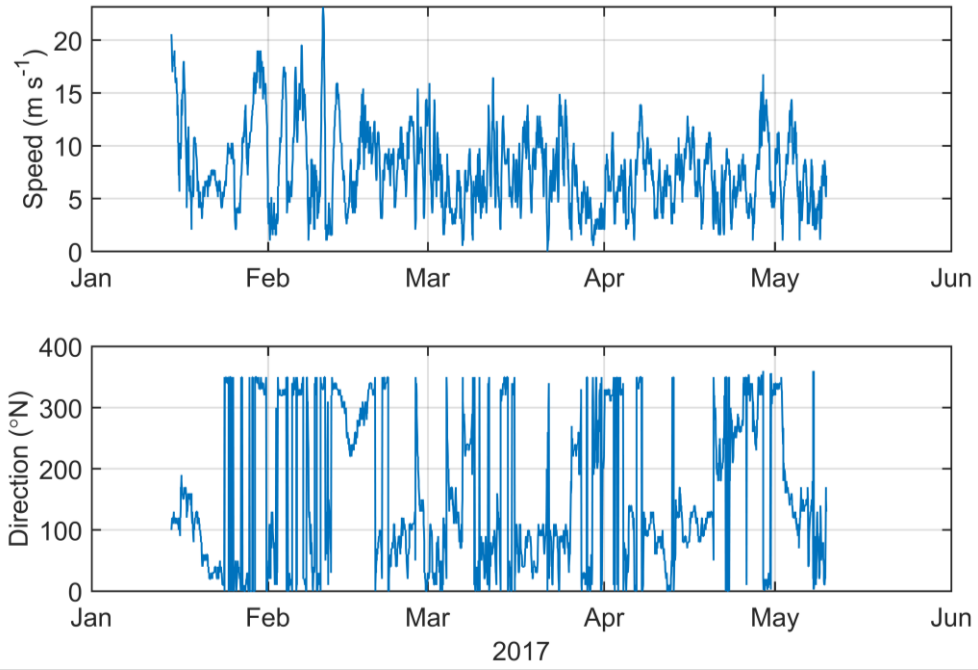

Figure 23. Hourly measured wind speed and direction from Tiree for the period 15th January – 6th May 2017. The direction data are in meteorological convention.

5.3.2 Flow Fields, 18th January – 5th May 2017

Modelled surface flows for 18th January – 5th May 2017 at the Macleans Nose site (Figure 24) are shown in Figure 25. Surface velocities are this location are parallel to the coastline, in a northwest to southeast orientation. Flow fields over a tidal cycle are shown in Figure 26. The velocity vectors highlight the spatially-varying nature of the flow at all stages of the tide.

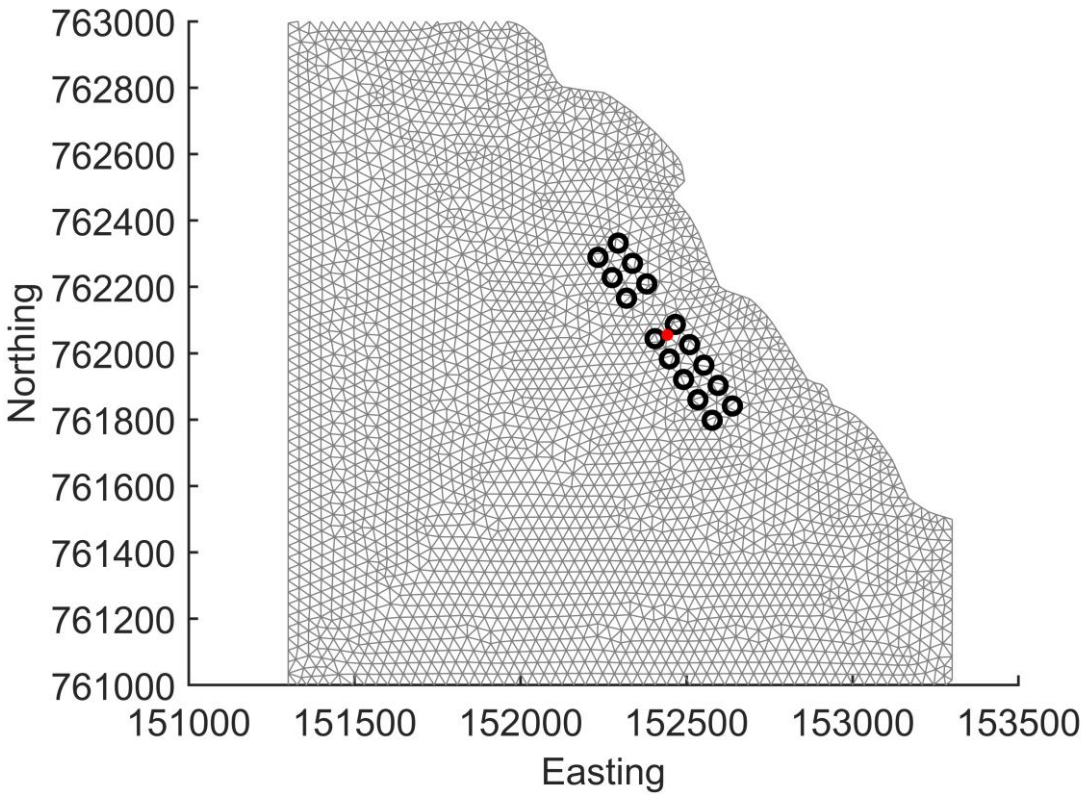

Figure 24. Location (•) of the modelled time series in Figure 25.

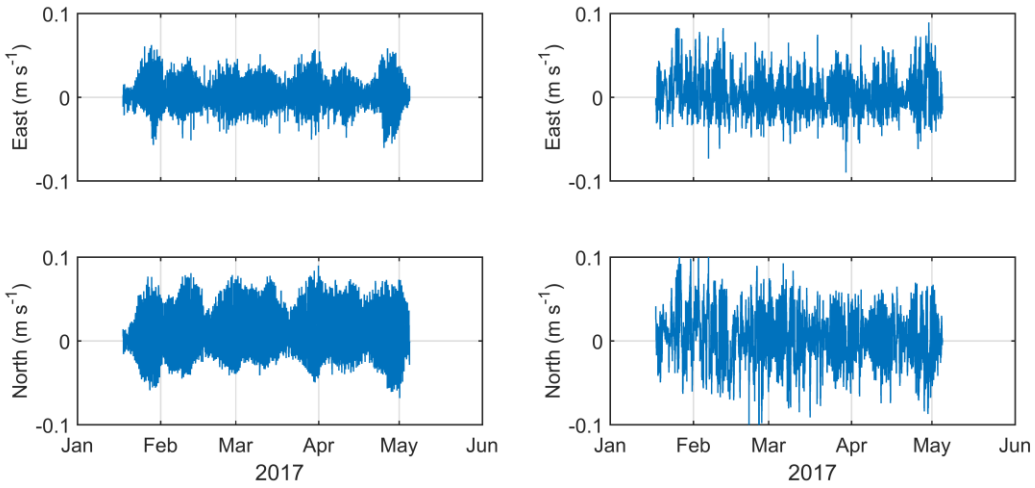

Figure 25. East (top) and North (bottom) components of the near-bed modelled flows, tide only (left) and full flow (right), for January – May 2017 at the Macleans Nose site (Figure 24). The time series length is 2568, corresponding to 107 days of hourly values.

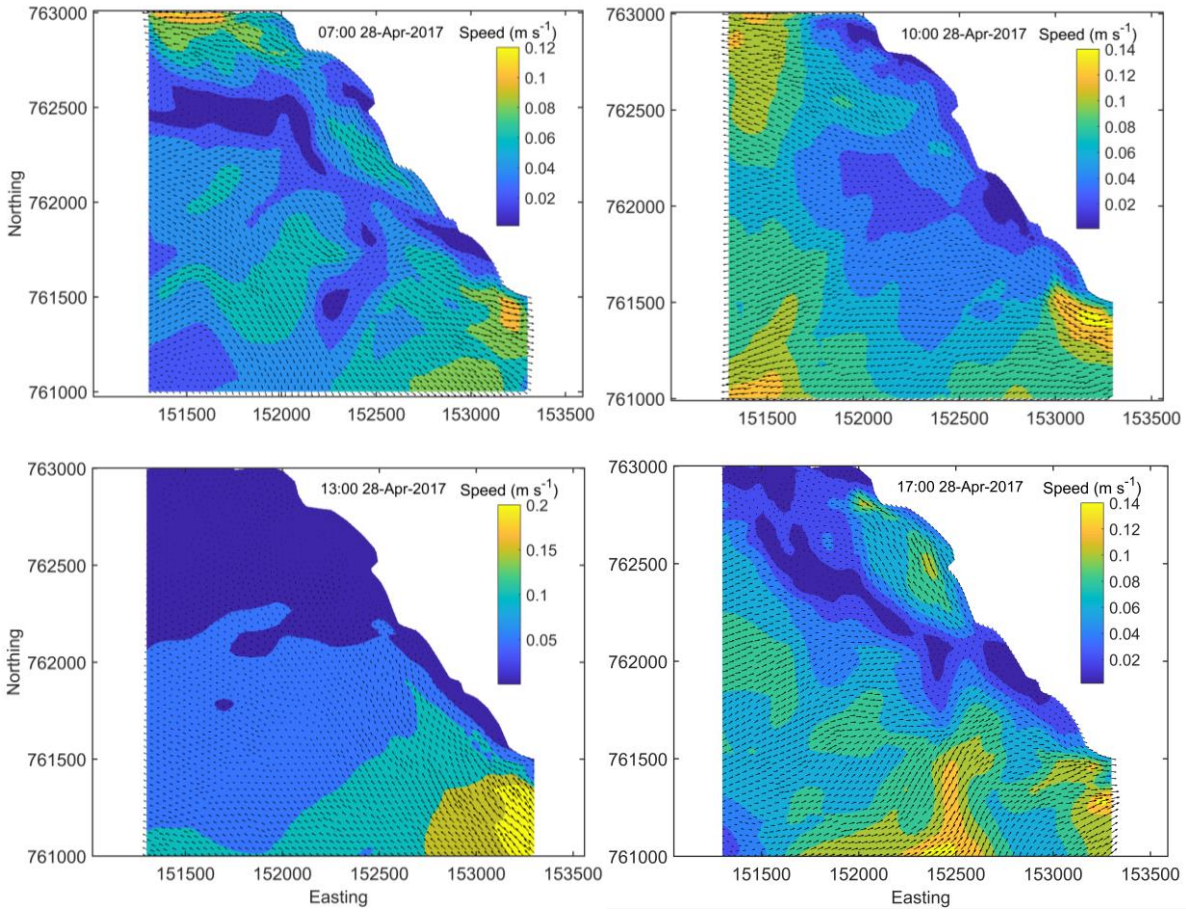

Figure 26. Modelled surface flow fields at intervals through a tidal cycle on 28th April 2017 (spring tide). The velocity vectors are superimposed on the coloured current speed. High water was at 07:15 on 28th April 2017.

The modelled surface mean current speed is shown in Figure 27. The mean speed decreases from South to North. In the vicinity of the cages, the mean speed was about 5 – 7 cm s^{-1}, similar to the measured values described in the hydrographic reports; near the bed, mean speeds were weaker, typically 2 – 4 cm s^{-1}.

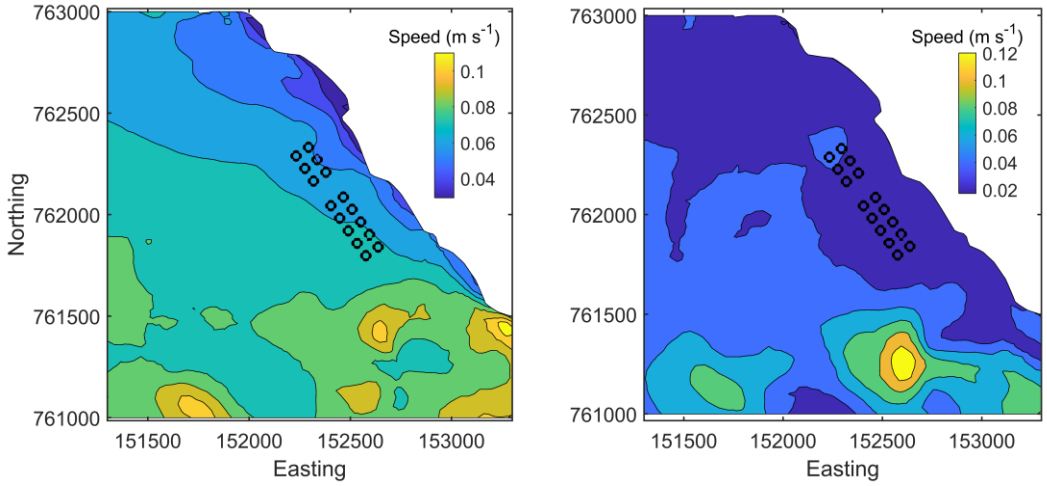

Figure 27. Modelled mean full flow current speed for surface (left) and nearbed (right) depths for January - May 2017.

5.3.3 Flow Fields, 30th October 2015 – 12th February 2016

Modelled flows for 30th October 2015 – 12th February 2016 at the Macleans Nose site (Figure 24) are shown in Figure 28. Only full-flow velocity fields were generated for this time period, since the flow fields were used to calibrate and validate NewDepomod, but not to forecast the footprint for the proposed biomass.

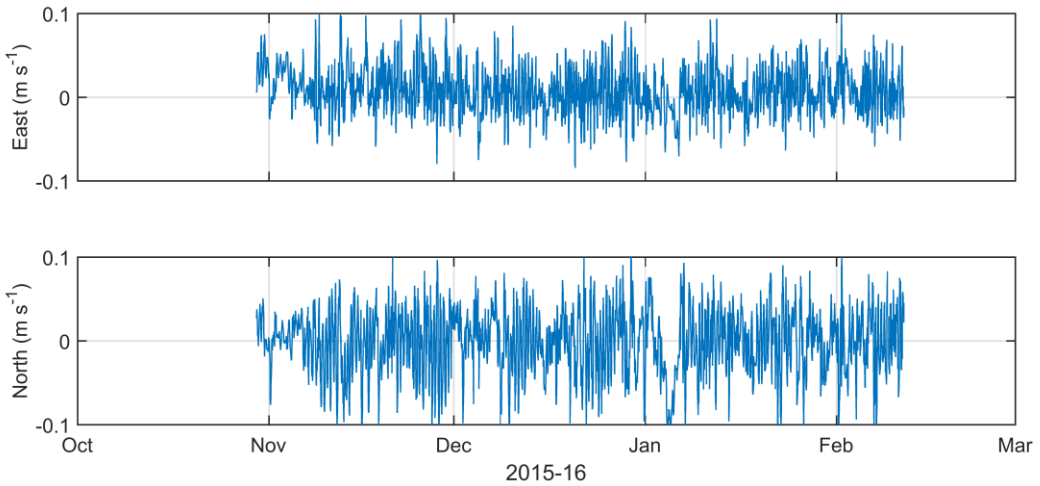

Figure 28. East (top) and North (bottom) components of the modelled flows, for October 2015 – February 2016 at the Macleans Nose site (Figure 24). The record length is 2520, corresponding to 105 days of hourly values.

The modelled surface mean current speed is shown in Figure 29. The mean speed decreases from south to north. In the vicinity of the cages, the mean surface speed is about 8 – 12 cm s^{-1}, similar to the measured values described in the hydrographic reports; the near-bed mean speeds were weaker, typically 4 – 5 cm s^{-1}.

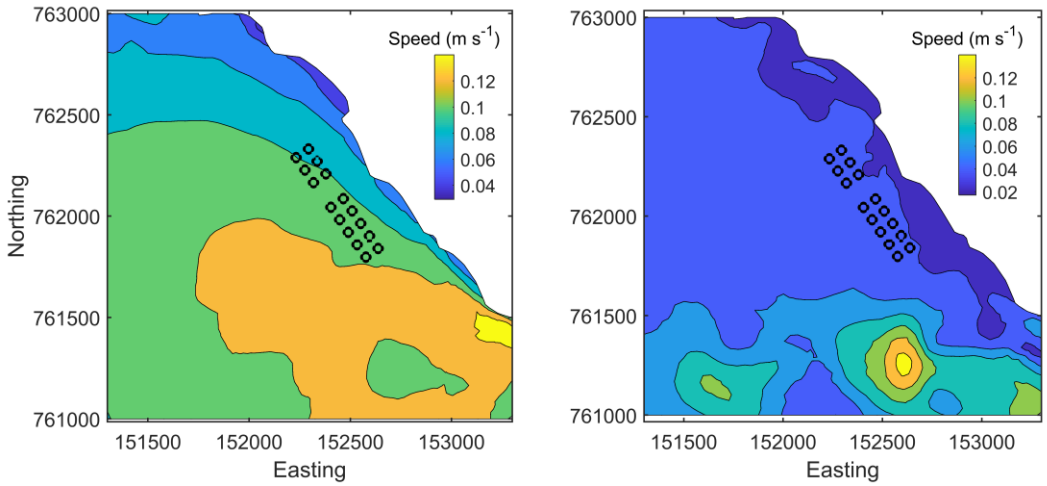

Figure 29. Modelled mean full flow current speed at surface (left) and near-bed (right) depths for October 2015 – February 2016.

5.3.4 Waste Feed and Faecal Solids

In order to obtain the best calibration and validation of NewDepomod, the waste feed and faeces inputs were derived from actual feed inputs, as recorded for all Marine Harvest sites

and archived in the AquaFarmer database. Waste feed was assumed to amount to 3% of the feed supplied. For the estimate of faecal pellet waste, we followed Wang et al. (2012). They suggested that feed water content was 4% and that 80% of carbon in the feed was absorbed by the fish. The remainder, amounting to about 19% of the feed supplied, was assumed to be discharged as faecal waste.

Time series of waste feed and faecal solids supplied to NewDepomod for the 2016 – 2017 and 2015 – 2016 simulations are shown in Figure 30 and Figure 30 respectively.

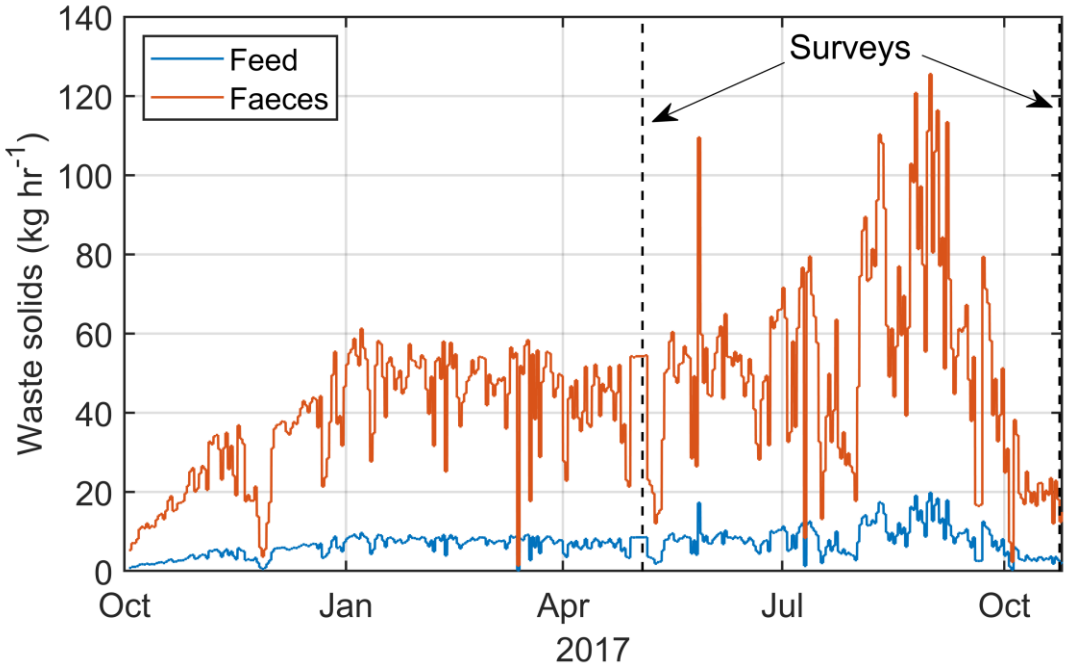

Figure 30. Time series of waste feed and faecal solids supplied to NewDepomod for the 2016 – 2017 production cycle. The times of seabed surveys are indicated.

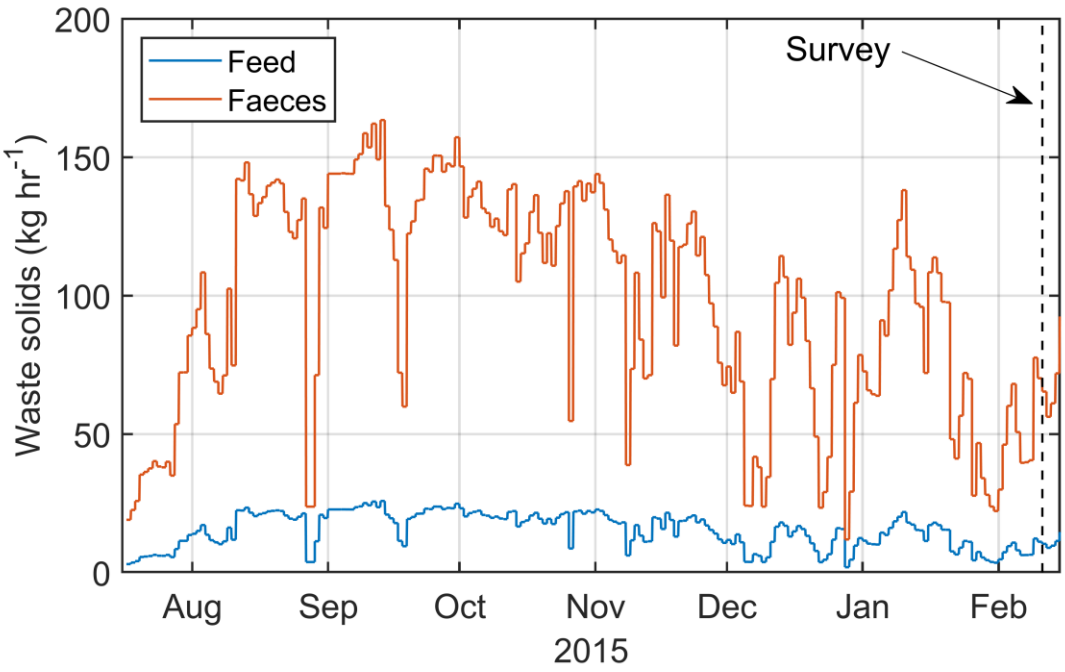

Figure 31. Time series of waste feed and faecal solids supplied to NewDepomod for the July 2015 – February 2016 simulation. The time of the seabed survey is indicated.

5.4 Calibration and Validation Results

5.4.1 Slice ("EMBZ")

Multiple simulations for Slice were performed, with varying NewDepomod parameter settings. The simulation that produced the best comparison against the available Slice residue data from the survey of 3rd – 4th May 2017 used the parameter values set out in Table 9. This simulation produced predicted concentrations of emamectin benzoate that were largely comparable with the observed values. The survey in May 2017 collected samples along four transects extending out from the cage groups, plus two reference stations (Figure 32). From these data, collected at seventeen locations in total, emamectin benzoate was only detected at two, stations 8 and 9 immediately to the north of the cage groups. *The objective of the calibration exercise, therefore, was to produce modelled concentrations of comparable magnitude to the observed values at stations 8 and 9, and low modelled values (preferably < 0.1 µg kg^{-1}) at all other sample locations*. Following numerous (several hundred) simulations, this was best achieved with the parameter set given in Table 9.

The observed and modelled concentrations of emamectin benzoate along a transect through the cages (Figure 32) illustrate the agreement between model and data. At stations 8 and 9, modelled concentrations were comparable to those observed, typically 0.5 – 1.0 µg kg^{-1}. At stations 3 – 7, to the south-west of the cage group, emamectin benzoate was not detected in the samples and modelled concentrations were very low (< 0.2 µg kg^{-1}). In between, directly beneath the cage group, modelled concentrations were significantly higher, but no data were available for comparison. Only station 10, along the south-western edge of the cage group was

sampled close to the transect shown: no emamectin was detected in the sample, and the modelled concentration was 0.46 µg kg^{-1}.

The value of dLayerMass = 478 kg allows some consolidation of sediment, particularly beneath the cages, but does not lead to rapid consolidation throughout the model domain. Using smaller values of dLayerMass led to rapid modelled consolidation of sediments, and therefore a persistence of emamectin benzoate outwith the cage area which was not found in the observations. Alternative parameter settings, such as reducing the expansionT50 coefficient, did not mitigate the persistence effect to the same extent as modifying the dLayerMass parameter.

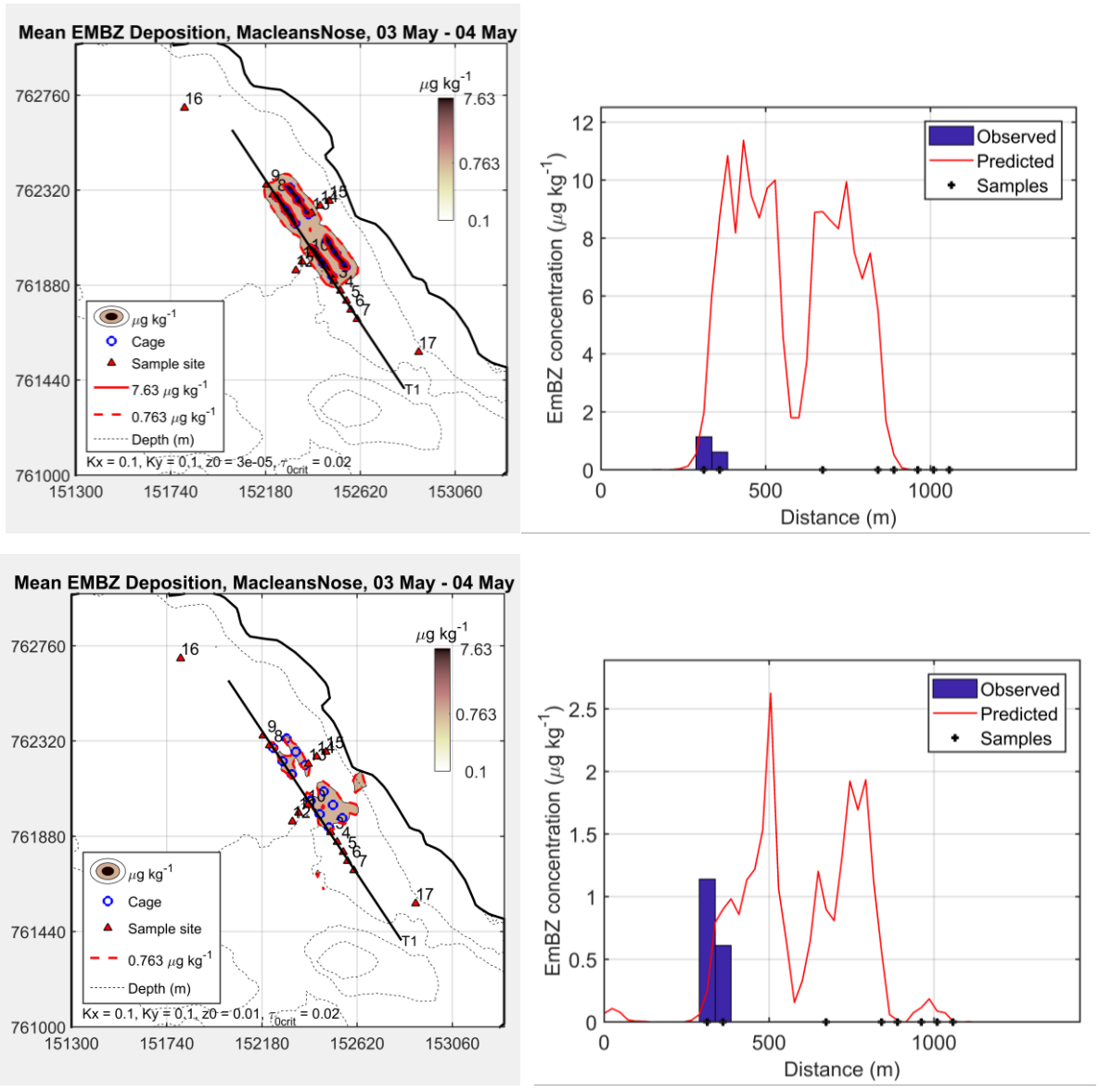

Figure 32. Results of the Slice calibration for the survey of 3rd – 4th May 2017. Results from the run with SEPA default parameter settings are shown on top, results from the calibration simulation on the bottom. The modelled concentrations and sample locations are shown on the left, and the modelled and observed concentrations along the transect indicated are shown on the right.

Table 9. NewDepomod parameter values that achieved the best calibration result. Values that are different from the SEPA default values are highlighted in bold.

Parameter	Value
Suspension X/Y dispersion coefficient (m^2 s^{-1})	0.1
Bed X/Y dispersion coefficient (m^2 s^{-1})	0.1
Resuspension X/Y dispersion coefficient (m^2 s^{-1})	0.1
Suspension Z dispersion coefficient (m^2 s^{-1})	0.001
Bed Z dispersion coefficient (m^2 s^{-1})	0.001
Resuspension Z dispersion coefficient (m^2 s^{-1})	0.001
Friction Velocity calculation	**Law of the wall**
Bed roughness (m)	**0.01**
Minimum erosion stress threshold (Pa)	0.02
Mass Erosion Coefficient	0.031
Bed Layer Mass (dLayerMass, kg)	**478**
Shear modified settling	OFF
Allow buoyancy	OFF

For validation, EmBZ simulations were repeated for July 2015 – February 2016, and compared with residue samples taken on 11th February 2016 (Figure 33). Only two samples were taken in February 2016, at both of which emamectin benzoate was undetected. The model, whilst predicting the presence of emamectin directly underneath the cages, correctly modelled the absence of emamectin at the sample locations.

A second validation simulation was conducted for October 2016 – October 2017, with model results compared to residue samples taken on 24th October 2017 (Table 8). As for February 2016, only two samples were taken, at the south-eastern end of the cage array, and emamectin was not detected. Again, the model predicted emamectin concentrations under the cages but correctly predicted the absence of emamectin at the sample locations (Figure 34).

Based on the EmBZ calibration and validation exercise, we take the parameter values from Table 9 and apply them to predictions of the benthic footprint.

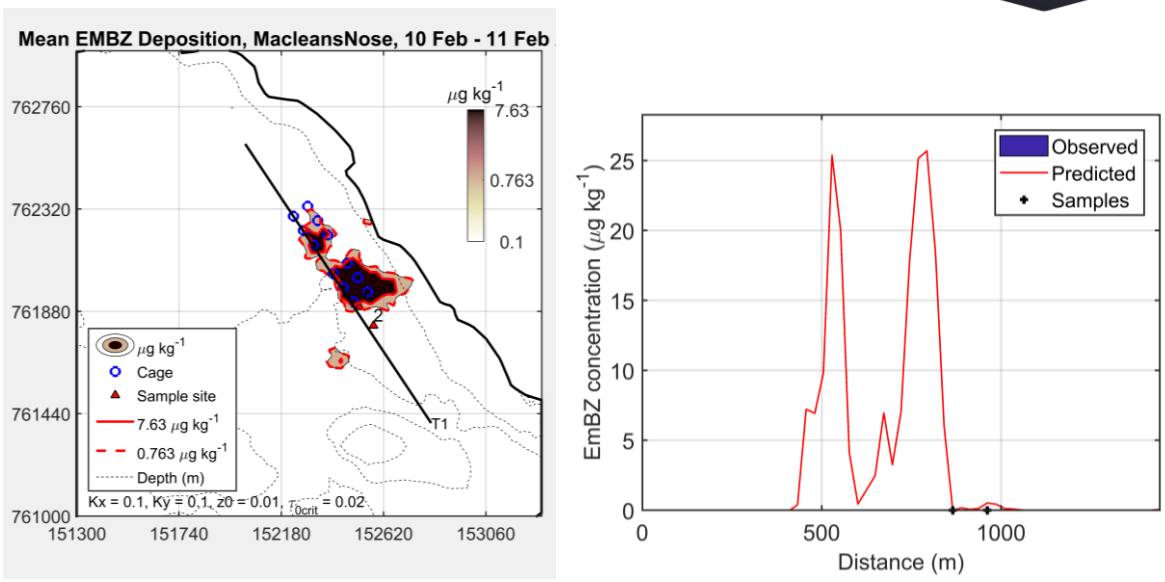

Figure 33. Results of the Slice validation for the survey of 11th February 2016. EmBZ concentrations are shown in plan view (left) and along the transect, from north to south (right).

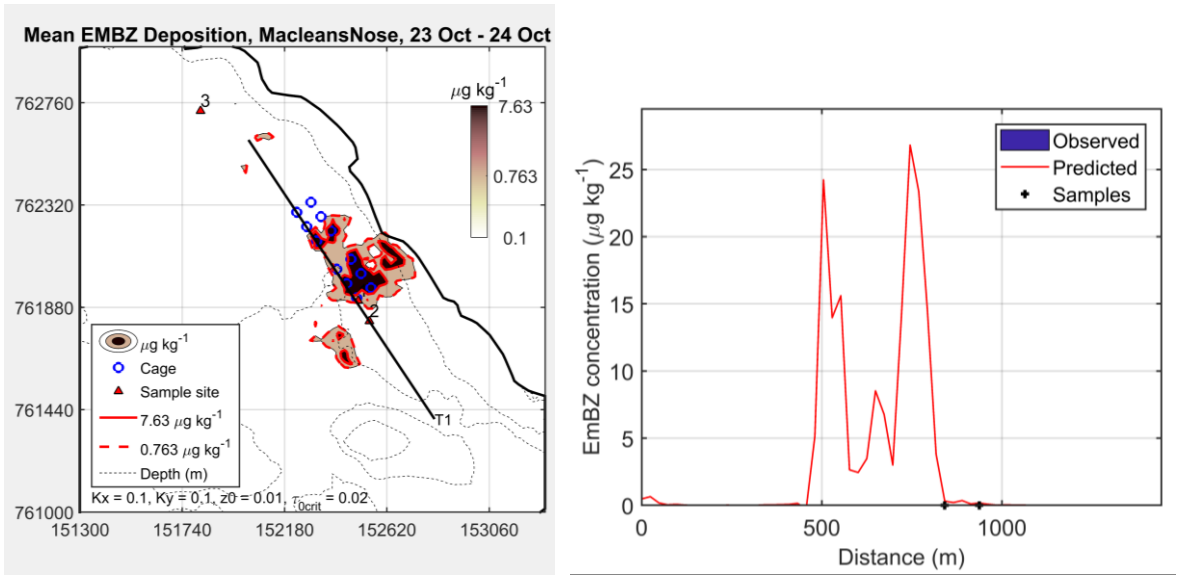

Figure 34. Results of the Slice validation for the survey of 24th October 2017. EmBZ concentrations are shown in plan view (left) and along the transect, from north to south (right).

5.4.2 Benthic footprint ("NONE"), October 2016 – May 2017

The objective of the calibration exercise for the benthic footprint was to establish a relationship between the modelled solids deposition and the observed metric of benthic quality, the Infaunal Quality Index (IQI). The IQI was determined for samples taken during a seabed survey in May 2017 (Table 10).

Benthic quality is thought to be influenced by both the intensity and duration of solids deposition beneath fish farms. In order to reflect both temporal and intensity aspects of the deposition, a percentile approach was taken to relate modelled deposition to observed IQI. With this approach, deposition over the entire model simulation is recorded at 3-hourly intervals over the whole model domain. At each sample location, the solids deposition which is exceeded for any specified percentage of time can be derived. For example, the 80th percentile of deposition over the simulation for October 2016 – May 2017 (Figure 35) is the rate of deposition that was not exceeded for 80% of the time. In other words, during the simulation deposition did exceed the rates shown, but for no more than 20% of the time. The use of percentiles, therefore, incorporates a temporal element into the relationship between modelled deposition and observed IQI.

For any simulation, any percentile of deposition can be modelled. For example, plotting the 100th percentile would be equivalent to plotting the maximum deposition that occurred during the simulation (since deposition is less than or equal to the maximum for 100% of the time). Plotting the 50th percentile is equivalent to plotting the median deposition that occurred during the simulation. For this report, we compared the 50th, 60th, 70th, 80th, 90th and 95th percentiles of deposition with the observed IQI and decided that the 80th percentile deposition rate was a suitable metric to use.

Table 10. Observed Infaunal Quality Index (IQI) values at Macleans Nose at 16 stations sampled during 3rd – 5th May 2017.

Station ID	Day	Month	Year	Easting	Northing	IQI
1	3	5	2017	152498	761898	0.74
2	3	5	2017	152528	761854	0.68
3	3	5	2017	152556	761807	0.77
4	3	5	2017	152576	761765	0.83
5	3	5	2017	152605	761723	0.87
6	4	5	2017	152214	762300	0.32
7	4	5	2017	152184	762344	0.86
8	4	5	2017	152390	762024	0.66
9	4	5	2017	152350	761989	0.68
10	4	5	2017	152321	761948	0.72
11	4	5	2017	152244	761878	0.78
12	3	5	2017	152395	762213	0.22
13	5	5	2017	152434	762248	0.83
14	5	5	2017	152476	762270	0.72
15	5	5	2017	151805	762702	0.76
16	5	5	2017	152891	761570	0.88

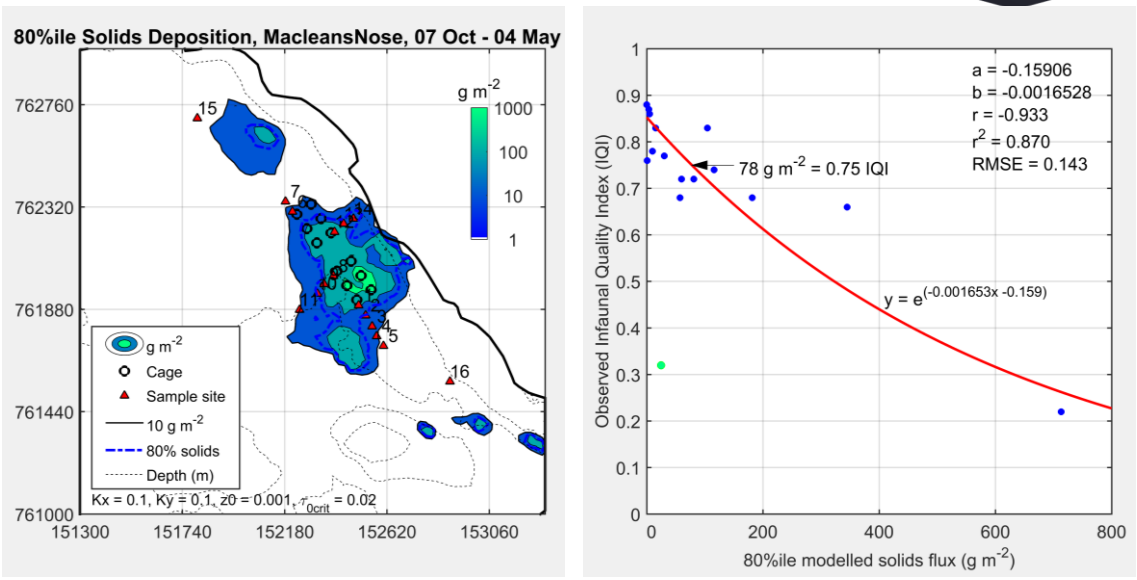

Figure 35. Results of the calibration for October 2016 – May 2017. The 80th percentile of deposition over the simulation period is shown with the sample locations indicated (left). On the right, the relationship between 80th percentile of deposition and the observed IQI is shown. The red line indicates the relationship between deposition and IQI used to forecast the future footprint. Note that deposition at Station 6 (green point) was poorly modelled, and that data point was not used when fitting the curve, but it was included when the errors (r2, RMSE) were calculated.

The predicted 80th percentile of deposition for October 2016 – May 2017 is shown in Figure 35. Modelled deposition was highest directly beneath the cage array, and extended southwards, consistent with the major axis of the near-bed velocity at the site. Observed IQI values at the sample locations exhibited relatively little impact along the northwest and northeast transects, where modelled deposition was low. Observed ITI values were lower to the south, close to the cages, where modelled deposition was highest. The overall relationship between modelled deposition and observed IQI was good (Figure 35). Deposition was poorly modelled at a single sample location, station 6 (IQI = 0.32), probably due to the hydrodynamic model slightly underestimating northward flow at the site. Based on Figure 35, the following relationship was estimated between modelled deposition and IQI:

$$\widehat{IQI} = e^{-(0.001653x+0.159)} \quad (1)$$

where x is the modelled deposition, and $\widehat{IQI}$ is the predicted IQI. The RMSE value in Figure 35 is the error between the observed and predicted IQI.

The relationship in Equation (1) predicts that an IQI greater than 0.75 will be achieved where deposition exceeds 78 g m^{-2} no more than 20% of the time (i.e. where deposition is less than or equal to 78 g m^{-2} for 80% of the time).

Note that when fitting the curve in Figure 35, deposition at Station 6 (green point) was excluded as deposition at that specific location was poorly modelled and including the data point skewed the relationship between deposition and IQI. However, the data point was included in the error (r2, RMSE) calculations (Figure 35).

The robustness of the IQI prediction equation was tested in the validation runs described in the next sections.

5.4.3 Benthic footprint ("NONE"), July 2015 – February 2016

The predicted benthic footprint for July 2015 – February 2016 is shown in Figure 36. This footprint is based on the relationship between the 80th percentile of deposition value of 78 g m^{-2}, defining the area where the IQI may fall below 0.75. Using Equation (1), values of IQI can be predicted based on the modelled deposition at the sample locations. The agreement with observed IQI on 11th February 2016 was good (RMSE = 0.032, r^2 = 0.97), although the number of data points is obviously limited.

Table 11. Observed Infaunal Quality Index (IQI) values at Macleans Nose at 6 stations sampled on 11th February 2016.

Station ID	Day	Month	Year	Easting	Northing	IQI
1	11	2	2016	152517	761899	0.46
2	11	2	2016	152584	761808	0.78
3	11	2	2016	152588	761794	0.83
4	11	2	2016	152590	761785	0.84
5	11	2	2016	151799	762713	0.84
6	11	2	2016	152892	761564	0.91

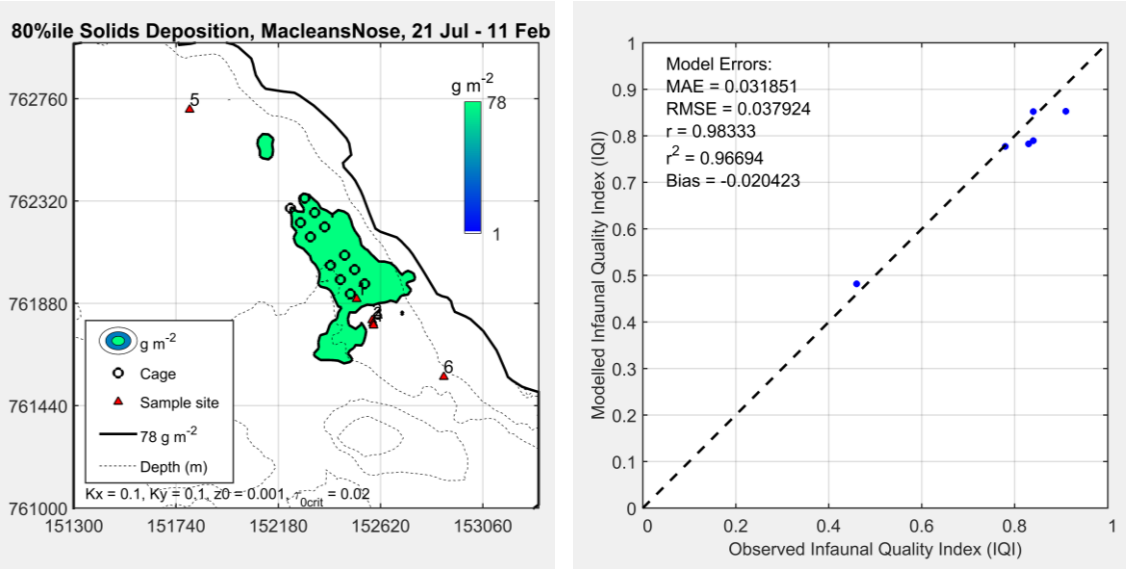

Figure 36. Modelled footprint, based on the 80th percentile of deposition (left), and predicted IQI against observed IQI (right) for February 2016.

5.4.4 *Benthic footprint ("NONE"), October 2016 – October 2017*

The predicted benthic footprint for October 2016 – October 2017 is shown in Figure 37. This footprint is based on the relationship between the 80th percentile of deposition value of 78 g m^{-2}, defining the area where IQI may fall below 0.75. Using Equation (1), values of IQI were predicted based on the modelled deposition at the sample locations. The agreement with observed IQI on 24th October 2017 was good (RMSE = 0.064, r^2 = 0.98), although the number of data points was again obviously limited.

Table 12. Observed Infaunal Quality Index (IQI) values at Macleans Nose at 6 stations sampled on 24th October 2017.

Station ID	Day	Month	Year	Easting	Northing	IQI
1	24	10	2017	152498	761910	0.46
2	24	10	2017	152554	761815	0.77
3	24	10	2017	152561	761806	0.77
4	24	10	2017	152570	761794	0.83
5	24	10	2017	151819	762726	0.84
6	24	10	2017	152893	761569	0.89

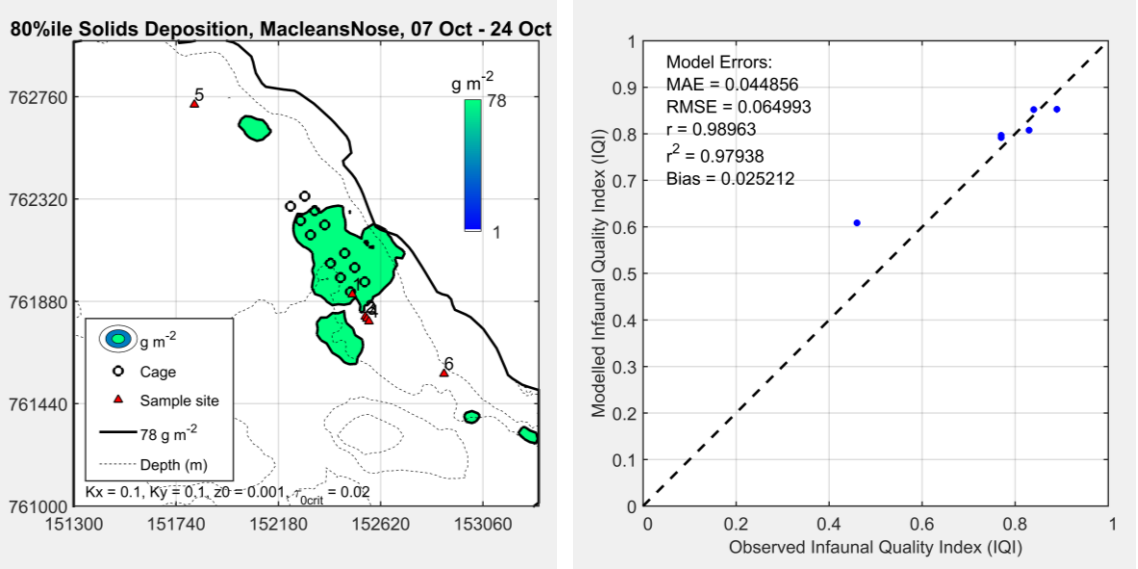

Figure 37. Modelled footprint, based on the 80th percentile of deposition (left), and predicted IQI against observed IQI (right) for October 2017.

6. NEWDEPOMOD FORECASTING

Based on the above, NewDepomod was applied to the fish farm site at Macleans Nose to predict the benthic footprint and potential Slice residues for an increased biomass of 3500 tonnes. The model was applied using flow fields from the hydrodynamic model described above. Following the Interim Guidance notes from SEPA (SEPA, 2018), NewDepomod will be used to make predictions for the following benthic and Slice scenarios:

1. A year-long simulation at the maximum proposed biomass using SEPA-recommended parameter settings (Kx = Ky = 0.1 m^2 s^{-1}; Kz = 0.001 m^2 s^{-1}; z0 = 3 x 10^{-5} m; shear-modified settling OFF; Allow Buoyancy OFF). Output from this simulation will be recorded at hourly intervals over the last 15 days of the simulations. For benthic simulations, the mean deposition over the 15-day period is considered the most important metric, given the likely delay in the response of the benthic faunal community to deposition rates; however, the minimum and maximum values of solids deposition will also be presented. This simulation will use the tide-only velocity field from the hydrodynamic model.

2. Simulation 1 will be repeated but using total velocity fields (i.e. tidal + non-tidal flows). Non-tidal flows will include the observed wind forcing from Tiree.

3. A 118-day long simulation of Slice dispersion and deposition for a treatment of the minimum (30 tonnes) and maximum (3500 tonnes) biomasses. Output from the model after 118 days will be presented. This simulation will use the tide-only velocity field from the hydrodynamic model.

4. Simulation 3 will be repeated but using total velocity fields (i.e. tidal + non-tidal flows). Non-tidal flows will include the observed wind forcing from Tiree.

5. Simulations 1 – 4 will be repeated using the parameter set in Table 9. Benthic results will be presented as the 80th percentile of deposition over the simulation period (one year at maximum biomass).

The results from the modelling exercise will be summarised in a NewDepomod Modelling Report submitted with the CAR application.

REFERENCES

Brickman, D., Ådlandsvik, B., Thygesen, U.H., Parada, C., Rose, K., Hermann, A.J. and Edwards, K. Particle Tracking. In: Manual of Recommended Practices for Modelling Physical – Biological Interactions during Fish Early Life, **2009**, pp. 27 – 42. Ed. by E. W. North, A. Gallego, and P. Petitgas. ICES Cooperative Research Report No. 295. 111 pp.

Burchard, H., 2002. Applied turbulence modeling in marine waters. Springer:Berlin-Heidelberg-New York-Barcelona-Hong Kong-London-Milan Paris-Tokyo, 215pp.

Chen, C., Lui, H., Beardsley, R.C. (2003), An unstructured, finite-volume, three-dimensional, primitive equation ocean model: Application to coastal ocean and estuaries, J. Atmos. Oceanic Technol., 20, 159–186.

Elliott A.E., P.A. Gillibrand and W.R. Turrell (1992). Tidal mixing near the sill of a Scottish sea loch. In Dynamics and exchanges in estuaries and the coastal zone, Coastal and Estuarine Studies, 40, D. Prandle (ed.), American Geophysical Union, Washington D.C., pp 35 56.

MSS, 2016a. The Scottish Shelf Model. Part 5: Wider Loch Linnhe Sub-Domain. Marine Scotland, available at: https://data.marine.gov.scot/dataset/scottish-shelf-model-part-5-wider-loch-linnhe-sub-domain

MSS, 2016b. The Scottish Shelf Model. Part 1: Shelf-Wide Domain. 5. Model Climatology. Marine Scotland, available at http://www.gov.scot/Publications/2016/03/8542/8

Pawlowicz, R.; Beardsley, B.; Lentz, S. Classical tidal harmonic analysis including error estimates in MATLAB using T_TIDE. Computers & Geosciences. **2002**, 28, 929-937.

SEPA, 2018. Regulatory modelling guidance for the aquaculture sector. Air & Marine Modelling Unit, 6th February 2018, 75pp.

Wang, X., Olsen, L. M., Reitan, K. I., and Olsen, Y. Discharge of nutrient wastes from salmon farms: environmental effects, and potential for integrated multi-trophic aquaculture. *Aquacult. Environ. Interact.*, **2012**, 2, 267–283. doi: 10.3354/aei00044

Wu, J. Wind-stress coefficients over sea surface from breeze to hurricane, J. Geophys. Res., **1982**, 87(C12), 9704–9706, doi:10.1029/JC087iC12p09704.